NTNU – Trondheim
Norwegian University of
Science and Technology

Acoustic and Elastic Impedance Models of Gullfaks Field by Post-Stack Seismic Inversion

Usman Shah Nawaz

Petroleum Geosciences
Submission date: September 2013
Supervisor: Egil Tjåland, IPT

Norwegian University of Science and Technology
Department of Petroleum Engineering and Applied Geophysics

Abstract

Gullfaks is one of the major hydrocarbon producing fields in the Norwegian continental shelf. This field has a quite complex geology which makes routine seismic interpretation a challenging task for understanding the reservoir properties such as lithology and fluid content. Post-stack seismic inversion has proven to be a reliable tool for detailed understanding of the reservoir especially for lithological identification.

In this study, post-stack seismic inversion method was used on acoustic and elastic impedance models to build an inverted impedance model. For this purpose, three horizons were interpreted from the reservoir zone to determine geological inputs for the model. Check shot survey was used to build synthetic traces which were then tied to the real seismic data. Two initial impedance models were then build i.e. acoustic initial impedance model and elastic initial model at zero degree angles. Four different inversion algorithms were applied to invert the initial models and their results were compared. The inverted models showed high vertical resolution with high signal to noise ratio, giving an excellent visualization of the reservoir zone.

Acknowledgment

All praise and thanks to Allah Almighty, Who bestowed me with focus, strength and patience to accomplish this study. I would like to convey my deepest gratitude to my thesis supervisor Dr. Egil Tjaland for his exceptional support, for sharing his knowledge and his valuable suggestions. Also, I would like to thank Mr. Knut Reitan Backe for his help in data loading into the software and assisting me in various ways.

Special thanks to the Statoil authorities for their cooperation and permission to use the data for the research. I greatly appreciate the policies of the Norwegian government and Department of Petroleum Engineering and Applied Geophysics for providing the quality education and making my stay an enriching and great experience.

Last but not the least: I would like to present my sincere gratitude to my parents for their unconditional love and motivation throughout my life. Special thanks to my family; for their encouragement and unwavering support.

Table of Contents

List of Figures

Chapter 1: Introduction

The development of structurally complex oil and gas fields requires a thorough understanding of reservoir characterisation in order to optimise the field performance. This requires integrated analysis and understanding of the available data such as seismic data and well log data. Seismic data provides important information about the general geology of the area. However, extracting geological information such as porosity, density and shale volume is a great challenge for an interpreter. In seismic studies, seismic inversion serves as one of the powerful tools s for estimating detailed characteristics of the reservoir. .

Different seismic inversion methods are used commercially to map the detailed reservoir properties such as lithology and fluid properties. These properties are estimated by using different inversion algorithms on the seismic data with prior geological knowledge and well log data. The relationship between seismic and lithology is empirical. The reduction of uncertainty in this relationship will have large effect on the reservoir model building, thus on development and production of the hydrocarbon (Badri et al., 2002). The inverted impedance model is also used for building facies and facies based porosity and permeability model (Shrestha et al., 2002).

In this research work, seismic algorithms are used on the seismic data from Gullfaks field, which is located on the western margin of the Viking Graben in the Norwegian North Sea. The post-stack seismic inversion was performed by integrating seismic data with well log data. Different inversion techniques such as Model Based, Bandlimited and Sparse Spike were used to create pseudo logs at each seismic trace location, to build a high resolution acoustic and elastic inverted impedance models. Since, the seismic inversion method converts the seismic amplitudes directly into the impedance values, special attention should be given to their preservation. Thus, the model built should be free of multiples, high signal to noise ratio and zero-off set migrated.

1.1 Project Workflow

The goal of this research project was to obtain detailed reservoir characterization such as reservoir rock properties and fluid parameters of the Gullfaks field. The work flow is organized as follows

- Interpretation of prominent horizons to get the prior knowledge of structure of the field.
- Building initial acoustic impedance model for different seismic inversion techniques to be applied.
- Applying various inversion techniques to invert the initial model for rock properties such as porosity and lithology.
- Analysis of inversion results.

This dissertation starts with the brief introduction of location of Gullfaks field in chapter 1. The general geology of the area is given in the chapter 2, the basic theory of seismic inversion is highlighted in chapter 3, the methodology followed during the research is elaborated in chapter 4 and lastly, the findings and discussion is presented in chapter 5.

1.2 Introduction to Area

The Gullfaks Field is situated south-east of the Statfjord Field and south of the Snorre Field in the northern North Sea, west of Viking Graben as shown in Figure 1.1. This field has been under production since 1986. Covering an area of 75 km^2, the field is developed by three platforms (Gullfaks A, B and C) under a fully Norwegian license group consisting of Statoil (operator), Norsk Hydro A.S. and Saga Petroleum A.S. Total recoverable reserves amount to about 365 x 10^6 Sm^3 of oil and some 23.10 x 10^9 Sm^3 of gas, located in the Jurassic Brent Group, Cook Formation and Statfjord Formation with remaining recoverable oil reserves about 11.6 x 10^6 Sm^3 (www.npd.no).

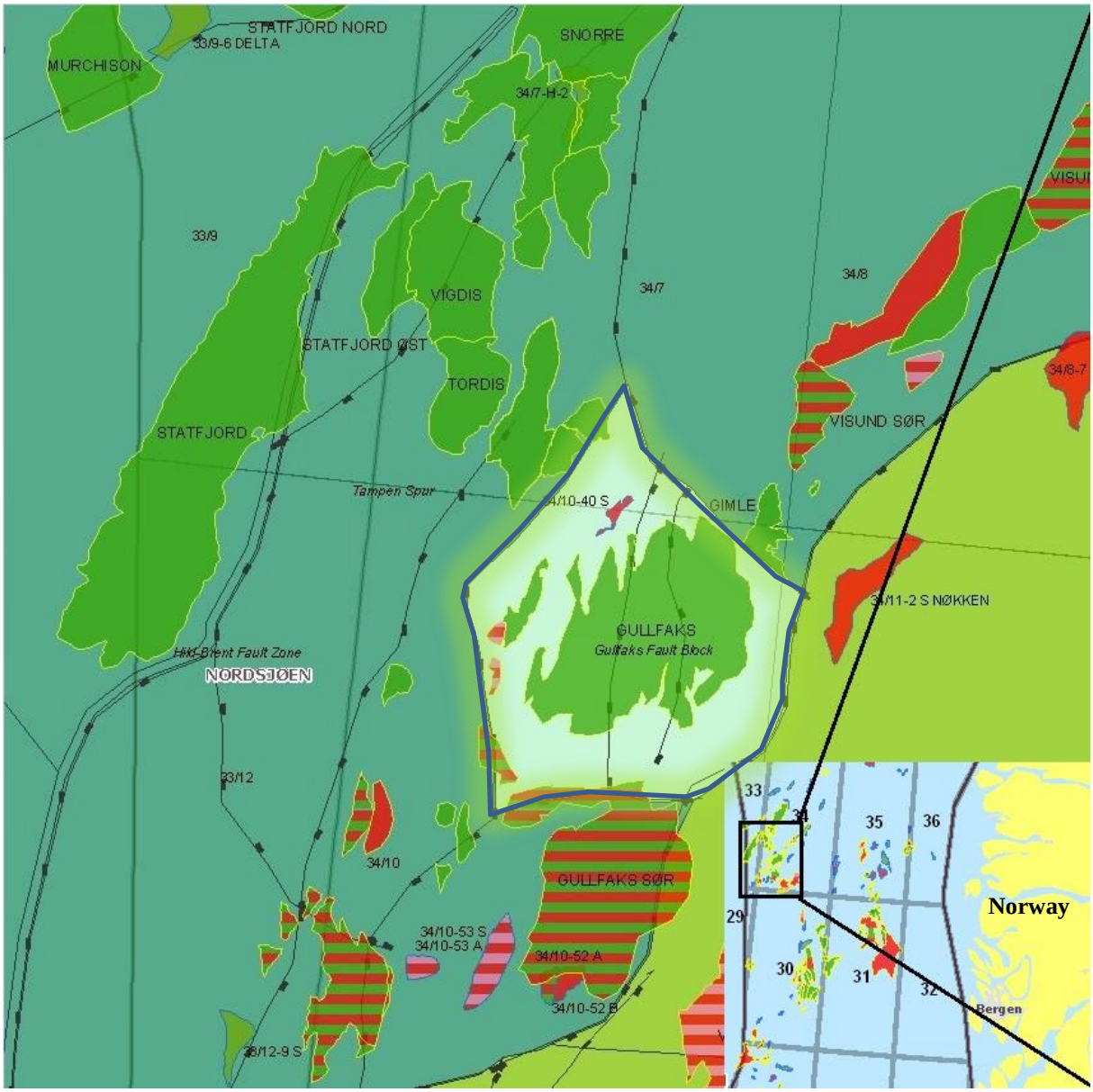

Figure 1.1: Regional map of Gullfaks field in the northern North Sea showed in highlighted area.

1.3 Data Available

The data provided for this research work includes 3D seismic cube and well log data. The seismic cube lies in the block 34 of the Norwegian continental shelf and it contains 1508 cross lines and 1099 inlines. The cross lines in the seismic cube are more or less oriented in north south direction and inlines are oriented in east west direction shown in the figure 1.2. The well data includes well logs and check shot surveys from wells 34/10-1, 34/10-3, 34/10-4 and 34/10-7.

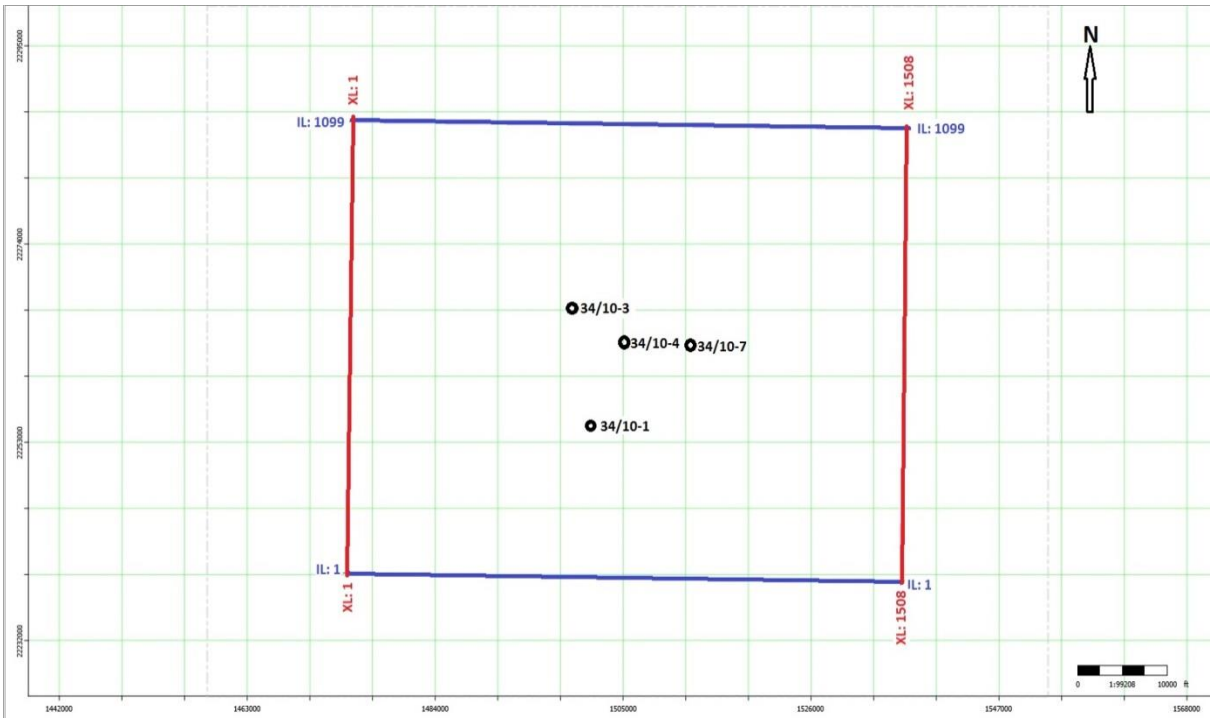

Figure 1.2: Base map of the Gullfaks field showing 3D seismic data cube and well positions.

Chapter 2: Geology of the area

2.1 Stratigraphy

The deepest well (34/10-13) was drilled to about 3350m depth in the Gullfaks area, and penetrated 1340m of Triassic sands and shales of the Lunde and Lomvi Formations (Hegre Group) shown in figure 2.1 (Erichsen et al., 1987). The base of the Triassic has never been reached in this part of the northern North Sea, and little is therefore known about early and pre-Triassic strata. From gravity surveys, palinspastic reconstructions and regional, deep seismic lines, it is, however, inferred that only thin sequences of sediments are present between the Triassic clastics and Devonian or metamorphic/crystalline basement in this area (Fossen, H and J.Hesthammer, 1998).

The Triassic Hegre Group consists of interbedded intervals of claystones, sandstones and shales, deposited in a continental environment. The upper part of the Hegre Group (the Lunde Formation) consists of medium-grained, fluvial sandstones and contains reserves in the eastern Gullfaks area. Overlying the Hegre Group is the Rhaetian-Sinemurian Statfjord Formation which consists of sandstones deposited in an alluvial environment that changed its character from a well-drained semiarid setting to a more humid alluvial plain (Fossen, H and J Hesthammer., 1998)

The thick Dunlin Group is subdivided into the Amundsen, Burton, Cook and Dark

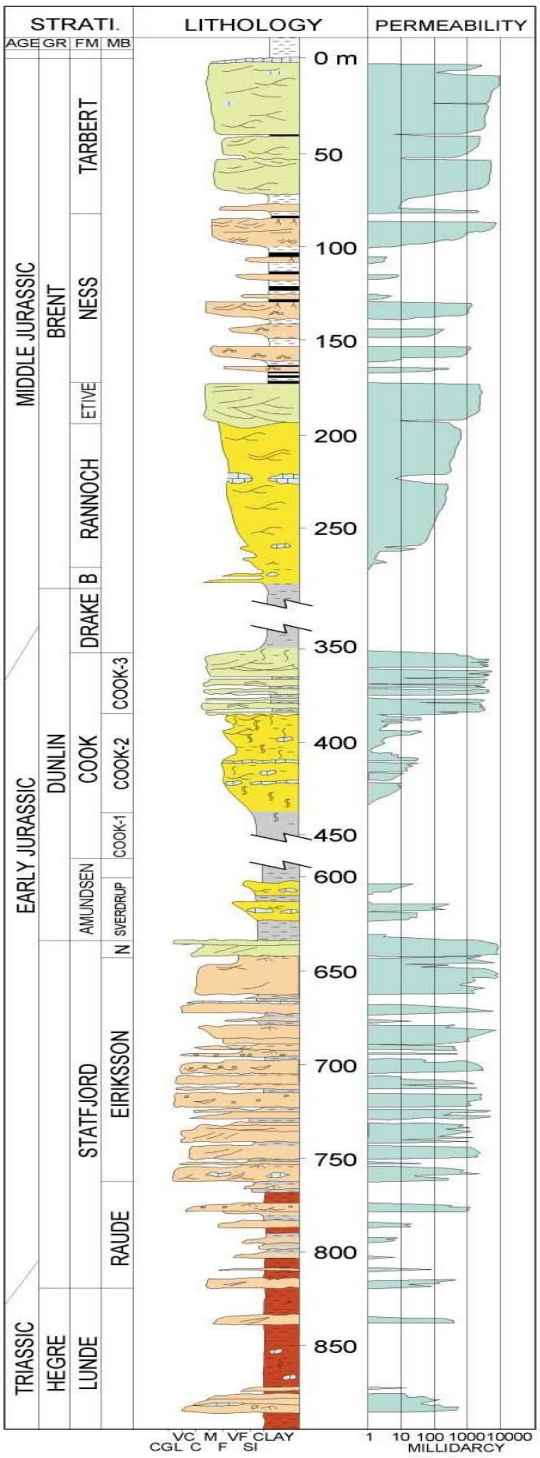

Figure 2.1: Stratigraphic column of Brent Delta (Hesthammer, J., & Fossen, H. 2001).

formations. The Amundsen and Burton Formations consist of marine claystones and siltstones overlain by the regressive, marine, silty claystones of the lower part of the thick Cook Formation, and in turn by muddy sandstones, sands and shales of the upper part of the Cook Formation. The thick Drake Formation comprises marine shales with varying amounts of silt.

The Brent Group of mainly Bajocian-Early Bathonian age forms the upper and main part of the reservoirs. It is sub-divided into the Broom, Rannoch, Etive, Ness and Tarbert Formations, all deposited in a deltaic environment. The vertical succession of the Brent Group is divided into two separate delta systems (Petterson et al., 1990).

- Lower Brent delta is interpreted as wave dominated delta system, which comprises Broom, Rannoch, Etive and Ness formations.

- Upper Brent delta is interpreted as tide dominated delta, which comprises Tarbet and Ness formation. A broad lithological sub-division can be made between the shaly Ness Formation and the sandy intervals below and above.

The reservoir rocks in the Gullfaks area are capped by the Cretaceous shales and siltstones. A major time gap (up to 100Ma) is represented by the base Cretaceous (late Cimmerian) unconformity on the Gullfaks Field, separating Upper Cretaceous sediments from Jurassic or Triassic sediments, and post-dating the major part of the faulting history of the area. Up to 100 m of Upper Jurassic shales (Heather Formation) are locally preserved in the hanging walls to the main faults in the Gullfaks Field, particularly in the western part (Petterson et al., 1990).

2.2 Structural geology of the area

The Gullfaks fault block is one of a series of large fault blocks in the North Sea shown in figure 2.2. The general trend (strike) of these large normal faults is N-S to NNE-SSW, reflecting the overall E-W extension across the rift. The extensional history of the North Sea starts from the Devonian extensional phase after the Caledonian collision (McClay et al. 1986). The main subsequent rifting phases are commonly referred to as the Permo-Triassic and late Jurassic phases (Badley et al. 1988; Gabrielsen et al. 1990). Significant extension involved in the Permo-Triassic event (Roberts et al. 1995), the late Jurassic deformation of the Jurassic sequence is more obvious on commercial seismic lines, and best known from well data.

The Gullfaks Field is characterized by two structurally contrasting compartments (Fig. 2.2): a western domino system with typical domino-style fault block geometry, and a deeply eroded eastern horst complex of elevated sub-horizontal layers and steep faults. These two regions are significantly different as far as structural development is concerned. Between the western and eastern regions is a transitional accommodation zone (graben system) which is identified as a modified fold structure.

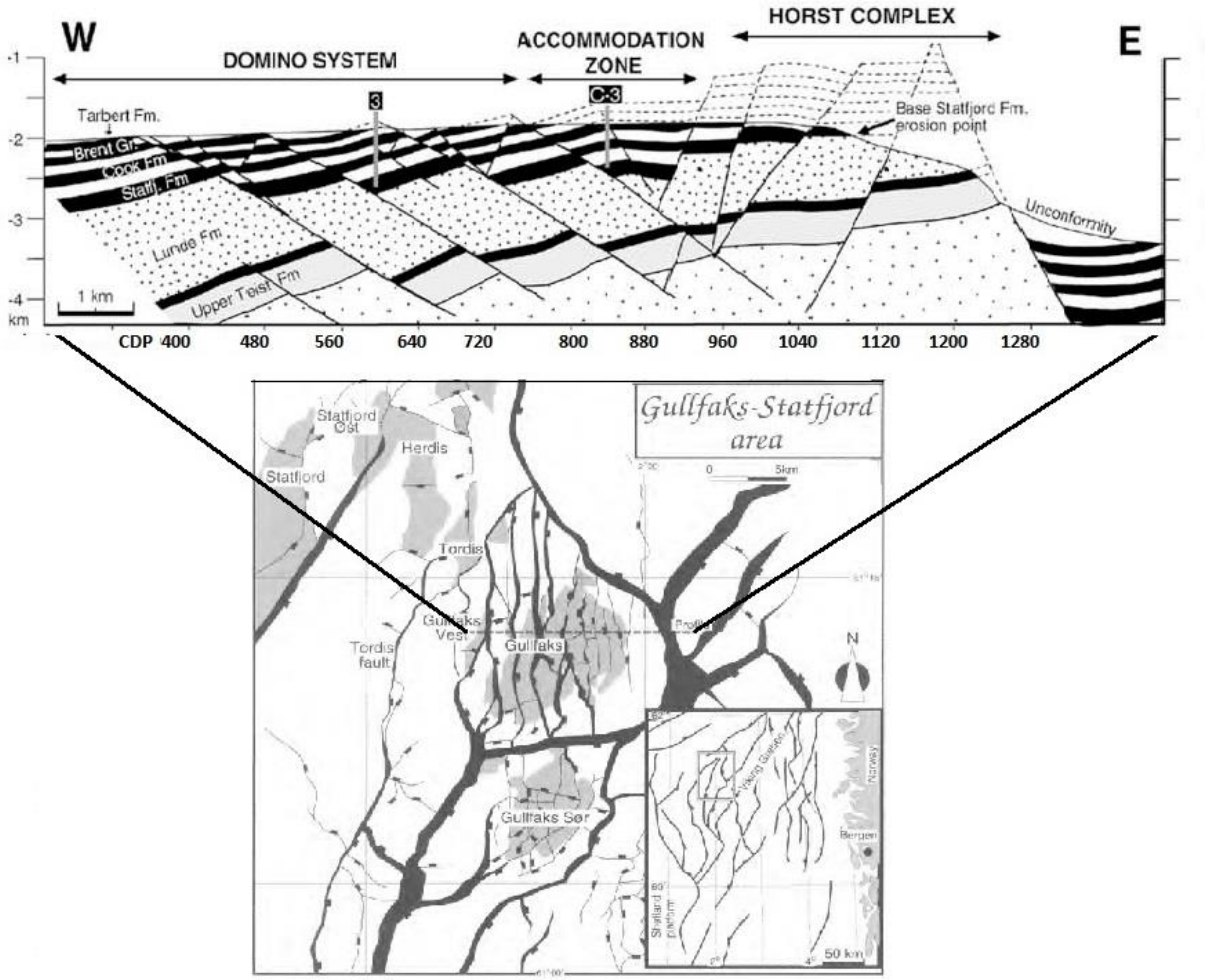

Figure 2.2: East-West profile across Gullfaks Field showing structural style of the area. (Modified from Fossen, H and J Hesthammer, 1998)

Seismic mapping has revealed a similar geometrical constellation on Gullfaks Sør to the south. The west-dipping domino faults exhibit displacement up 500 m. The fault dips 25-30^{o} to the east, whereas the bedding has an average dip of 15^{o} to the west. The faults show increasing complexity towards higher reservoir levels. Several E-W trending minor faults with offsets less than 50 m compartmentalise the domino fault block, and are believed to be related to the internal block deformation during differential slip along the main faults (Fossen & Rørnes, 1996).

The poor quality of the seismic data because of horst complexes complicates the interpretation. Bedding with the horst complexes is mainly sub-horizontal or gently east-dipping. The accommodation zone (Figure 2.2) is bounded by the steep (65^{o}) faults to the east and lower-angle (25^{o}) faults to the west. The zone is identified as collapsed zone anticline with a west-dipping western limb and a sub-horizontal eastern limb. (Hesthammer, J., & Fossen, H. 2001).

2.3 Petroleum geology

There is a little doubt that sediments of Upper Jurassic to lowermost Cretaceous age, particularly that of the Kimmeridge Clay Formation are the source of vast bulk of hydrocarbons in the Central and Northern North Sea.

It is difficult to obtain good-quality seismic data from Gullfaks Field because of following reasons:

- The presence of gas in post-Jurassic section results in high absorption, hence poor signal penetration.
- The two horizons top Paleocene and top cretaceous are very strong reflectors, therefore a low proportion of original seismic energy penetrates the pre-cretaceous section.
- These two reflectors also generate strong multiples, which interfere with pre-cretaceous reflections.
- Low seismic reflectivity of these layers may also be the cause of poor seismic quality in pre-cretaceous section.

Following horizons have been mapped at the reservoir:

Base of cretaceous;
Top of Brent Group in the western part of the field;
Top of Statfjord formation;

The improved quality of data acquired in 1979 has resulted in more accurate and complete structural interpretation. (Erichsen, T., Helle, M., Henden, J., & Rognebakke, A. 1987).

2.3.1 Traps

The Gullfaks structure represents the most positive element of the Tampen Spur, which limits the Viking Graben along its western and north-western edge. The seismic interpretation shows the Gullfaks Field as a westerly dipping fault block system consisting of small fault blocks oriented mainly N-S. The trap is characterised as a structural trap comprising many rotated and later partly eroded fault-blocks.

The main reservoirs are Jurassic sandstones with upper Jurassic shales as source rock. Sealing is provided Cretaceous shales. The oil is trapped mainly in Brent sandstones which are 250 m thick in the uneroded part. The oil-water contact in the Brent sandstone is 1947 mss, in the cook formation at 2090 mss and 2043 mss in the Statfjord Formation. Gas-bearing sands have been encountered at the depth of 300-450mss in strata of Pliocene age. The thickness of the sand varies from 1-5 m and the areal extent seems to be 6-8 km^2 for the most important interval.

(Erichsen, T., Helle, M., Henden, J., & Rognebakke, A. 1987).

2.3.2 Reservoirs

The main reservoirs in Gullfaks area lie in the Brent Group of middle Jurassic age specifically early Bajocian-early Bathonian age. Older reservoirs like Cook Formation of Dunlin Group and Statfjord Formation are also important as a reservoir.

(Erichsen, T., Helle, M., Henden, J., & Rognebakke, A. 1987).

2.3.2.1 Statfjord Formation

The formation is normally divided into three units (Figure 2.3) and represents a gradual upward transition from an arid alluvial environment to a poorly drained alluvial plain with channelized flows. Finally, a transgressive low-energy shoreline advanced across the area.

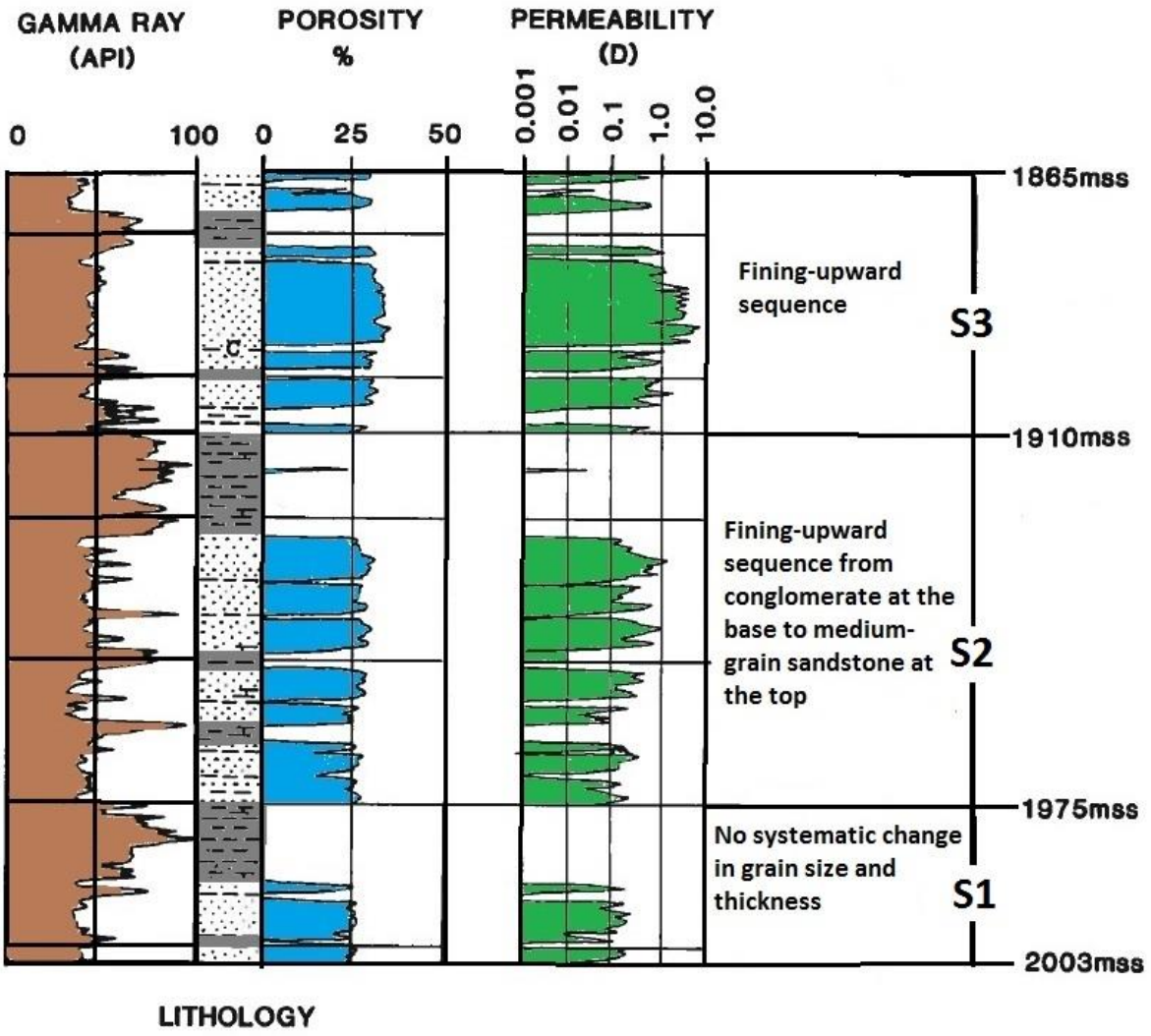

Figure 2.3: Statfjord reservoir, Well 34/10-11 (modified from Erichsen, T. 1987).

All three units contain interbedded sandstones, siltstones and shales. Unit 1 appears to be random with no obvious systematic change in grain size or bed thickness. In unit 2 and 3 fining upward sequences have been observed. Each sequence consists of smaller sab sequences grading from conglomerate and very coarse sandstone at the base to medium-grained sandstones at the top. Locally the sandstones are cemented. The porosities and

permeabilities average 19-30% and 30-3000mD respectively in the sandstones (Erichsen, T. 1987).

2.3.2.2 Cook Formation

Cook Formation of Dunlin Group plays an important role as a reservoir. It belongs to the Jurassic, argillaceous, marine sequence. The formation is divided into two units (Figure 2.4), which consist of sandstones, siltstones and shales deposited under both marine and restricted marine conditions in units 1 & 2 respectively. Four sedimentary facies have been recognized within the formation: (1) laminated sand and shale, consisting of interlaminated very fine sandstone and siltstone, (2) bioturbated muddy sand consist of very fine to fine grained sand in clay matrix, (3) hummocky sands with minor shale, (4) interbedded fine to medium grained sandstone with shale or siltstones. (Erichsen, T., Helle, M., Henden, J., & Rognebakke, A. 1987).

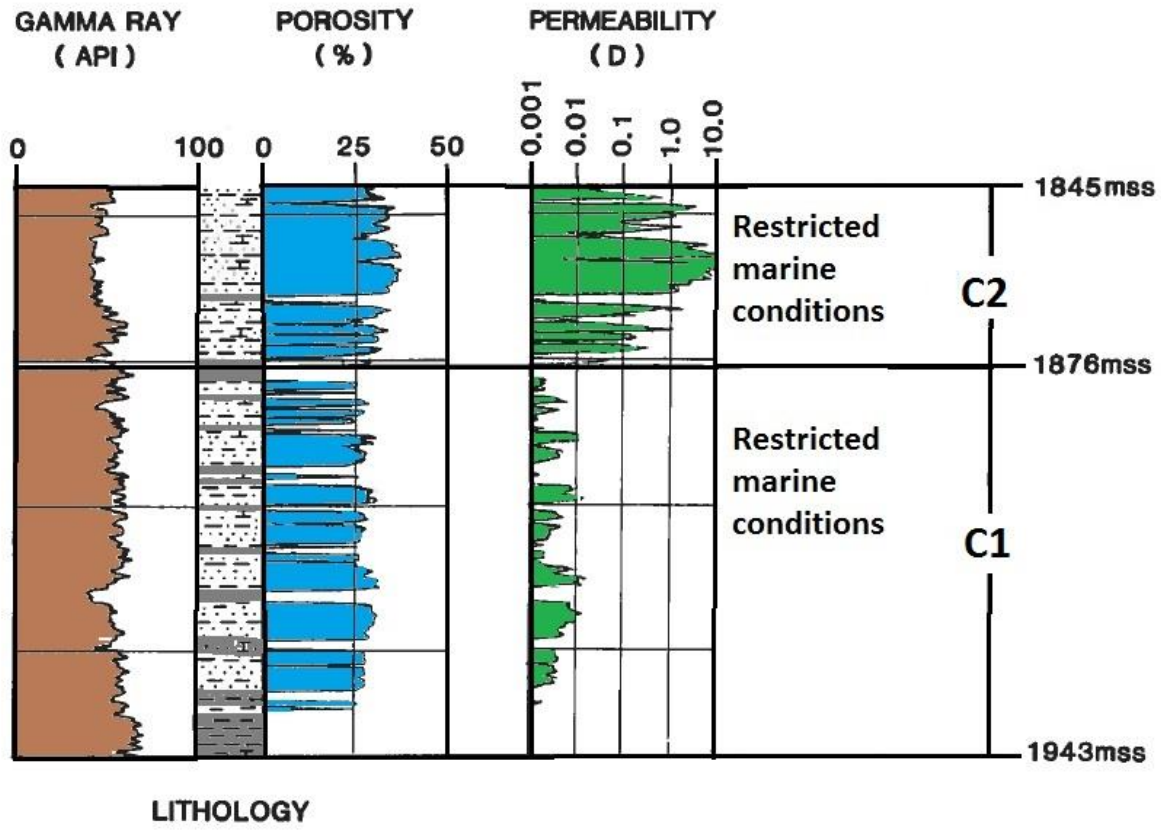

Figure 2.4: Cook reservoir, Well 34/10-5 (modified from Erichsen, T. 1987).

The sandstones are mostly arkosic in composition with cemented carbonate layers. Despite this the overall effect of diagenesis on poro/perm properties is minor. The porosities range from 20-36% whereas permeabilities are in the range of 1-1000mD (Erichsen, T. 1987).

2.3.2.3 Brent Group

The Brent Group is divided into five different formations, among which four formations Tarbert, Ness, Etive and Rannoch are important as reservoirs.

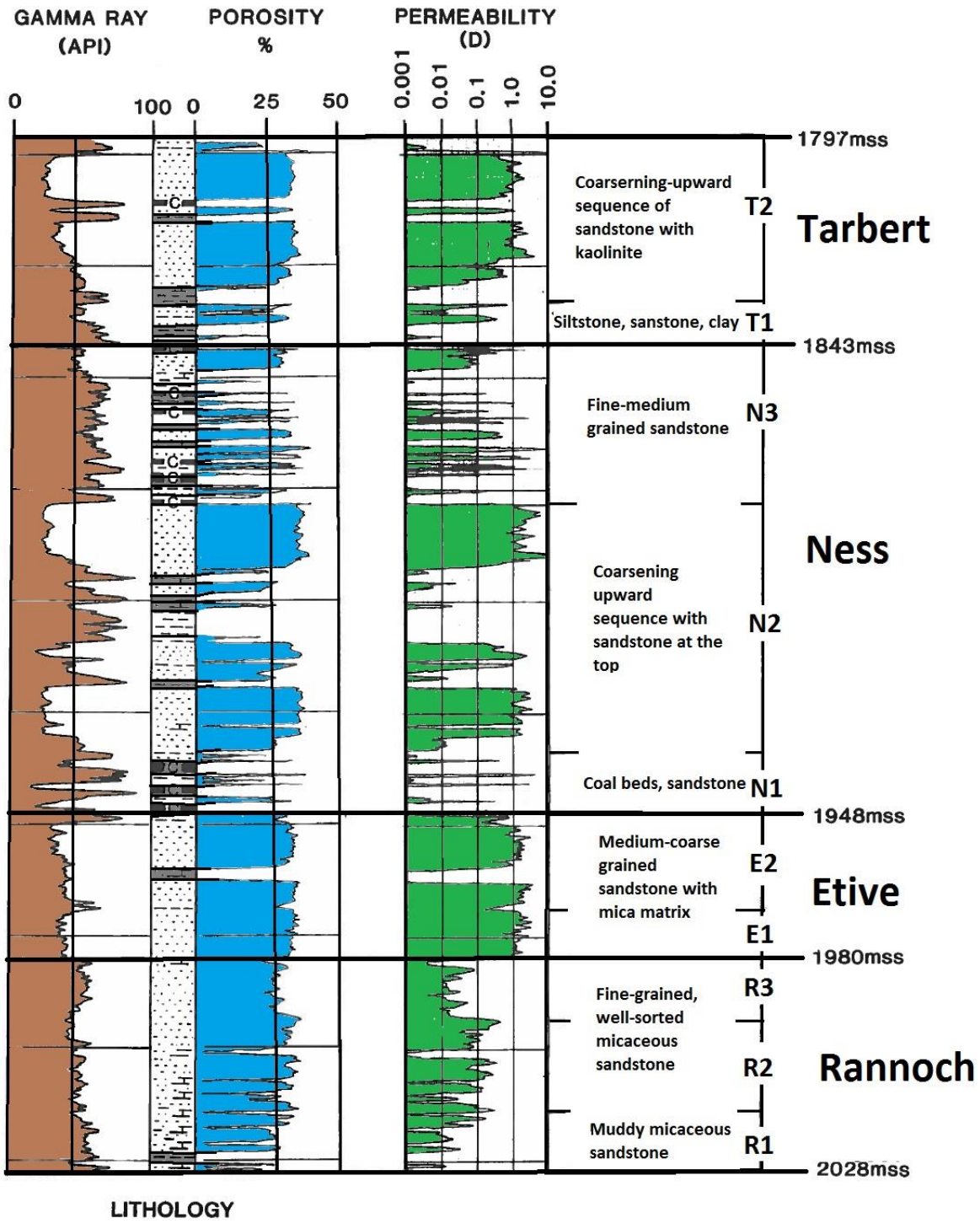

Figure 2.5: Brent Reservoir, Well 34/10-8 (modified from Erichsen, T. 1987).

2.3.2.3.1 Rannoch Formation

The Rannoch Formation is interpreted as a delta-front deposit, comprising of an overall upward-coarsening sequence which gets thin towards south. The formation is subdivided into three reservoir units: R1, R2, and R3 (Figure 2.5). R1 is muddy micaceous sandstone. R2 and R3 are dominated by very fine to fine, well-sorted micaceous sandstones. The average porosity is 30% and permeability ranges from 50-800mD (Erichsen, T.1987).

2.3.2.3.2 Etive Formation

The Etive Formation is interpreted as an upper delta-front complex. The formation is subdivided into two units: E1 and E2 (Figure 2.5). The unit E1 contains upward sequences which can be channel deposits, whereas well-sorted sandstones of unit E2 are interpreted as beach deposits. The formation has very good reservoir quality and contains predominately medium to coarse grained sandstones with minor clay and mica matrix. The average porosity is 32% and permeability range of several darcies (Erichsen, T. 1987)..

2.3.2.3.3 Ness Formation

The Ness formation is subdivided into three units: N1, N2, and N3 (Figure 2.5) representing delta-plain depositional environment. Units N1 and N2 represent the lower delta plain facies, whereas N3 represents the upper delta plain facies. Lower part of N1 consists of coal beds with rootlets and interbedded sandstones and mudstones, and upper part consists of thicker sandstone beds interpreted as fluvial channel-fill deposits. The N2 unit is interpreted as an interdistributary bay-fill deposit, and consists of coarsening-upward sequence with high porous and permeable sandstones on the top of sequence. Major characteristics of Unit N3 are soil profile, coal beds and siderite. Flood plain deposits, fluvial channel-sands and lacustrine deposits. The fine to medium grained sandstones of the fluvial channel deposits has porosity above 25% and permeability up to one darcy (Erichsen, T. 1987).

2.3.2.3.4 Tarbert Formation

The Tarbert Formation is subdivided into two units: T1 and T2, represents a transgressive event building up the upper Brent delta. These units are interpreted as a tide/fluvial dominated delta system: The Unit T1 consists of two or three coarsening-upward sequence ranging from bioturbated clay and siltstone at the bottom to medium to coarse gained sandstones at the top. The lower part of the Unit T2 consists of coarsening-upward sequence. Despite of secondary kaolinite in the sandstones, both units have very good reservoir properties (Erichsen, T. 1987).

2.3.3 Source

Geochemical analysis performed on different wells in the area indicates the main source rock lies within the Draupne Formation. This formation is 200-300 thick in Viking Graben and partly eroded on the structural highs. The total organic content shows 5-10% TOC in the Viking Graben. Shales and coals in the Brent Group are the other potential rocks, but their volume is restricted. Another possible source rock is the dark marine shales of the Dunlin Group. Maturity of the Dunlin Group is low but it is anticipated that it has generated hydrocarbons in the deeper parts of the basin. The Dunlin shales have limited oil potential but as good as gas potential (Erichsen, T. 1987).

Direct migration of hydrocarbon from the source-rock to the reservoir has probably contributed to the oil-filling of the Gullfaks structure because of the major fault towards the east and south. The major contribution of hydrocarbons to the Gullfaks seems to be have been taken place by the spilling of oil from other structures in the area, most probably from the structures Snorre ‘Vest’ and 33/9 Alpha (Statfjord Øst) (Erichsen, T. 1987).

Chapter 3: Basics of Post-Stack Seismic Inversion

3.1 General

The interest in seismic inversion techniques has been growing steadily over the last couple of years. Integrated studies are essential to hydrocarbon development projects and inversion is one of the means to extract additional information from seismic data. The main objective of seismic inversion is to transform seismic data into a quantitative rock property, descriptive of the reservoir. Inversion results show higher resolution compared to the working with seismic amplitudes and support more accurate interpretations. This in turn gives better estimations of reservoir properties such as net pay and porosity. An additional benefit is that interpretation efficiency is greatly improved (Pendrel, J. 2001).

The change in the subsurface lithology is represented by the relative change in acoustic impedances. Acoustic impedance is the physical property of the rock, unlike the seismic reflection data which is interface property, given as the product of density and velocity. Well logs measure both these properties directly, so by multiplying density and sonic log, acoustic impedance log is obtained. These acoustic impedance logs can be converted to the reservoir properties. Different seismic inversion schemes play an important role in seismic interpretation, reservoir characterization, time lapse seismic and other geophysical applications.

Seismic reflection amplitude information can be used to invert for, the relative impedances of the materials on both sides of the interface. So, special attention should be paid during seismic data processing to preserve the actual amplitudes related to the geological variations. Best inversion results can be obtained from seismic data without multiples, acquisition imprints and numerical effects, high signal/noise ratio and zero-offset migrated. Also, due to the band limited nature of the seismic data, lack of low frequencies will prevent the transformed impedance trace from having the basic impedances or velocity structure, crucial to making a geological interpretation (Shrestha et al., 2002).

Different types of inversion are performed on different types of traces. The main difference is between inversion performed before stacking and inversion performed after it, called pre-stack and post-stack inversions. Most seismic surveys provide images using data that have been stacked. Stacking is a signal enhancement technique that averages many seismic traces. The traces represent recordings from a collection of different source-receiver offsets with a common reflecting midpoint. Each trace is assumed to contain the same signal but different random noise. Stacking gives high signal to noise ratio and signal amplitude, equal to the average of the signal in the stacked traces. The resulting stacked trace is taken to be the response of a normal-incidence reflection at the common midpoint (CMP) (Barclay & Roberts, R. (2007).

When velocity of the overlying strata vary gradually and average amplitudes in the stacked data are equivalent to the amplitudes recorded in the normal incidence trace then post-stack inversion is performed. On contrary, when the amplitudes vary strongly with offset, pre-stack inversion is performed, and gives more clear geological features which post-stack seismic

inversion fails to differentiate. We will focus only on post-stack inversion as only full stacked seismic data is available.

3.2 Theories behind Post-Stack Seismic Inversion

The basis of all the inversion analysis is the input data. For the post-stack seismic inversion, stacked seismic volume and the well logs including velocity and density log is required. Thus, it is necessary to understand the basic phenomenon involved in creation of seismic data and it's relation with the rock physics. Measuring rock parameters with the help of seismic data and well logs can lead us to actual rock properties necessary for the reservoir characterization. The basic convolution model of seismic trace and the basics of the rock physics are discussed as follows.

3.2.1 Convolution Model of Seismic Trace

The seismic data is recorded in the time domain. The seismic waves with certain frequency are sent to the subsurface and recorded back at the surface giving the seismic trace. This measures the travel time from source to receiver. The convolution model of seismic trace contains three components: reflectivity, wavelet and noise. And it states that seismic trace is the convolution of earth's reflectivity with a seismic source function with addition of noise component. The equation is given as follows

$$s(t) = w(t) * r(t) + n(t) \quad \ldots\ldots\ldots\ldots\ldots\ldots\ldots\ldots (1)$$

Where:

s(t) = seismic trace
w(t) = seismic wavelet
r(t) = earth reflectivity
n(t) = noise
t = time

If we apply Fourier transformation on equation 1 we get the seismic trace in the frequency domain (equation 2), shown as follows

$$s(f) = w(f) \times r(f) \quad \ldots\ldots\ldots\ldots\ldots\ldots\ldots\ldots\ldots\ldots (2)$$

Where:

s(f) = Fourier transform of s(t)
w(f) = Fourier Transform of w(t)
r(f) = Fourier transform of r(t)
f = frequency

In the equation 2, it can be observed that in frequency domain convolution becomes multiplication. Fourier transform is a complex function and it is normal to consider the amplitude and phase spectra of the individual component (Latimer et al., 2000).

3.2.2 Reflection Coefficient

The reflection coefficient (reflectivity) is one of the basic physical concepts in the seismic methods. The reflection coefficient is the response of seismic wavelet to subsurface lithological changes given by acoustic impedances, which is defined as the product of density and velocity of the strata. Mathematically reflectivity or reflection coefficient is given as difference of acoustic impedances of two layers divided by the sum of acoustics impedances of the same layers, given below

$$R = (\rho_2 V_2 - \rho_1 V_1) / (\rho_2 V_2 + \rho_1 V_1) = (Z_2 - Z_1)/ (Z_2 + Z_1) \ldots\ldots (3)$$

Where:

R = reflection coefficient
ρ = density
V = compressional velocity
Z = acoustic impedance
1 and 2 are layers above and below the boundary

The main objective of the seismic inversion is to estimate the physical parameters of the subsurface layers i.e. density and velocity (P & S-wave) of the layers. From the stacked seismic data we can only estimate the P-wave acoustic impedance because stacked seismic data is zero-offset data. The relation between the zero-offset data and reflectivity is given in equation, where Z_1 and Z_2 are the acoustic impedances of layer 1 and layer 2 respectively. The recursive inversion is used to estimate the acoustic impedance, which is often referred as trace integration. From equation 3 acoustic impedances can be expressed as:

$$Z_2 = Z_1 (1+ R) / (1-R) \ldots\ldots\ldots\ldots\ldots\ldots\ldots\ldots (4)$$

Where:

Z_1 = acoustic impedance of layer 1
Z_2 = acoustic impedance of layer 2
R = reflectivity

The equation 4 gives the recursive equation by which acoustic impedance can be obtained as a function of two-way travel time. It can be obtained by using most advance inversion algorithms, often combined with the use of well logs. In the seismic trace obtained, it is assumed that there is no multiple energy and that absorption effects have been removed (Latimer et al., 2000).

3.2.3 Seismic Wavelet

In the convolution model, reflectivity is convolved with the wavelet donated as w(t) to get the seismic traces called synthetic seismic. The wavelet is both complex in shape and it is time varying. Therefore estimation of seismic wavelet is critical in seismic processing and interpretation of the reflection seismic data. A brief description and characteristics of some wavelets are given below.

3.2.3.1 Minimum Phase Wavelet

According to Treit and Robison (1966), minimum phase wavelet is defined as for a given set of wavelets, all with the same spectrum, the minimum phase wavelet is the one which has sharpest leading edge i.e. wavelet with positive time values. It is important because the typical wavelet in dynamite work is close to minimum phase. The minimum phase has no component prior to zero time and energy is concentrated as close to the origin as possible.

3.2.3.2 Ricker Wavelet

The Ricker wavelet consists of a peak and two side lobs or troughs. The Ricker wavelet is dependent on its dominant frequency i.e. the peak frequency of its amplitude spectrum or inversion of dominant period in the time domain. Two Ricker wavelets are shown in the figure 4.4 with high and low frequency. The amplitude spectrum of the wavelet is broadened as the wavelet gets narrow in the time domain, indicating an increase in resolution. The ultimate wavelet would be a spike with a flat amplitude spectrum (Mondol, N, H., 2003).

The wavelet shown in the figure 4.4 is zero phase or symmetrical wavelets. The energy is concentrated at the positive peak of the wavelet, which give better resolution when convolve with the reflectivity. Frequency is also an important parameter; high frequency wavelet gives good resolution comparatively to the low frequency wavelets (Mondol, N, H., 2003).

3.2.4 Noise Component

The recorded seismic traces are not the true representative of the subsurface lithological boundaries but also contain some unwanted signals. These unwanted signals are called noise. The seismic noise is grouped into two broad categories: random noise and coherent noise.

The noise which is due to environmental factors and uncorrelated with the traces is called Random Noise e.g. noise due to moving vehicles. And the noise which is predictable on the seismic trace but unwanted is called Coherent Noise e.g. multiples. The random noise is an additional component n(t) shown in equation 1. By stacking the data this noise can be removed. The seismic energy that has reflected more than once in its travel path is called multiples. They may be very easy to recognize or extremely complex as interbedded multiples. They can be partially removed by stacking but require more powerful processing steps such as deconvolution, f-k filtering and inverse velocity stacking to be fully removed (Mondol, N, H., 2003)

3.3 Rock Physics

Apparently inversion seems to have very simple goal of determining density, P and S-wave velocities for calculating acoustic impedances. However this simple process is complicated by the two problems.

- How to get these parameters unambiguously
- How to infer lithology from physical parameter

To solve these problems we first need to look at the simple rock model, which consists of matrix and pores filled with fluid shown in figure 3.3. Figure shows that velocity and density

can be affected by (1) type and shape of the matrix, (2) porosity of the rock and (3) type of fluid filling the pores.

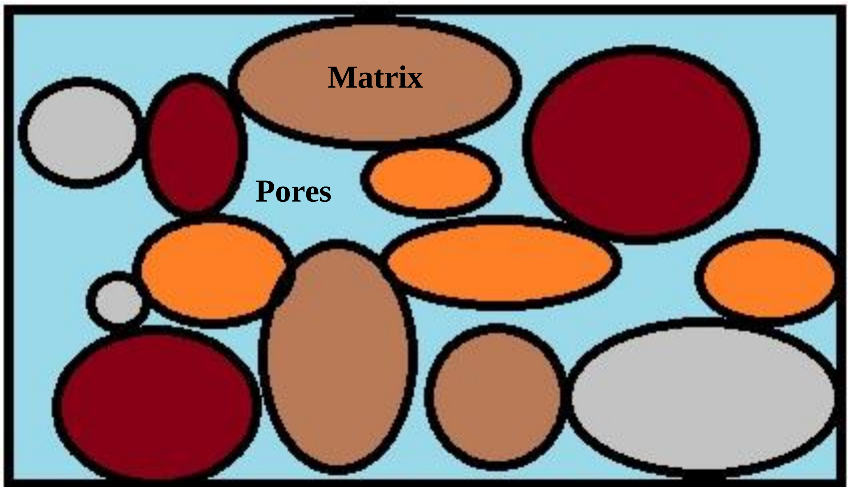

Figure 3.1: Simple rock model with matrix and porosity shown by blue colour.

For simplicity if we assume that there is single matrix type and two fluids filling the pores (oil and gas), Wyllie's equation can be used to determine the density as.

$$\rho_b = \rho_m (1- \phi) + \rho_w S_w \phi + \rho_{hc}(1- S_w)\phi \text{ ....(5)}$$

Where ϕ is the total porosity, Sw is the water saturation, ρ_b is bulk density of the rock, ρ_w is the density of water and ρ_{hc} is the density of hydrocarbons. From the above equation it is noted that bulk density of the rock is very much dependent upon the fluid filled in the pores. In the gas reservoirs density decreases dramatically which play a very important role is the interpretation of the reservoir.

And for determining the velocity equation 5 can be written as

$$1/V_b = (1 - \phi)/V_m + S_w\phi/V_w + (1-S_w)\ \phi/V_{hc} \text{ .... (6)}$$

Where ϕ is the total porosity of the rock, S_w is water saturation, V_b bulk velocity, V_w is the velocity in water, V_m is the matrix velocity and V_{hc} is the velocity of the hydrocarbons.

3.3.1 Relationship between P-wave velocity and density

The density can be estimated from P-wave velocity (V_p) and vice versa using empirical relationship known as Gardner's equation. It is a pseudo-velocity relationship commonly used in estimating sonic or density logs when only one of them is available which are used during well tie. For the density Gardner equation is given as

$$\rho = \alpha\ V_p^{\beta} \text{ .... (7)}$$

Where ρ is density, Vp is P-wave velocity and α and β are empirical derived constants that depends upon the geology. Gardner et al. proposed that one can obtain a good fit by taking $\alpha = 0.23$ and $\beta = 0.25$. Assuming this, the equation (7) is reduced to:

$$\rho = (0.23)Vp^{(0.25)} \text{ ..... (8)}$$

Lindseth (1979) proposed an empirical relation between acoustic impedance and density which is used to extract the density from the reflectivity, given as:

$$V = \alpha (\rho V) + \beta \text{ ..... (9)}$$

Where $\alpha = 0.308$ and $\beta = 3400$ ft/s were empirical derived values from Lindseth (1979).

3.4 Basic Inversion Methodology

The post-stack seismic inversion is a processing technique which aims to extract acoustic impedance information from stacked seismic data. In principle it is quite straightforward and involves the convolution and vertical incidence reflection coefficient equation (1). The equation suggests that if we are able to remove or reduce noise component, deconvolve the wavelet and restore the original amplitudes, we are only left with earth's normal incidence reflectivity which is related to acoustic impedance given as equation (4).

Practically it is impossible to exactly recover the reflection coefficient from the seismic trace and there will be always amplitude, noise and residual wavelet problems. There are two inputs to post-stack seismic inversion, which is stacked seismic data and a model of geological constraints. These are combined to produce the final inversion closely depending upon the algorithm used.

Bandlimited inversion involves direct integration of seismic data to produce bandlimited inverted seismic trace and then deriving the missing low frequency trend from the geological model. The sparse-spike inversion method estimates a set of sparse reflection coefficient from the seismic data, constraining the reflection coefficients with the model and then inverting the coefficients to produce the impedance. Model-based inversion starts with the initial geological model and then this model is adjusted until the synthetic seismic section best fits the acquired seismic data.

(Russell & Toksöz et al, 1991)

Chapter 4: Project Methodology

This project was carried out in several steps which include:

- Software and Data Loading
- Well to Seismic Tie
- Initial Model Building
- Inversion Techniques Applied
- Generating 3D Model

4.1 Step 1: Software and Data Loading

The software package Geoview under Hampson Russel software suit was used for this study. The Hampson Russel software is known for encompassing all the aspects of seismic exploration and reservoir characterization, from AVO analysis and seismic inversion to 4D multicomponent interpretation (www.cgg.com). Geoview serves for two purposes: (1) acts as a well-log data base and (2) to run other programs such as Elog and Strata. The Elog is used to perform functions on logs such as log editing, smoothing and log correlation while the Strata is used to perform pre-stack and post-stack inversions, AVO and attribute analysis etc.

For this project, data available included well logs in addition to check-shot surveys of wells 34/10-1, 34/10-3, 34/10-4 and 34/10-7 and 3D stacked seismic cube. The first step of post-stack seismic inversion process is to load the well locations in the Geoview data. The base map of the area with available wells and geographical orientation of the seismic cube is shown in the figure 2.2. After loading the data, the log curves and check-shot surveys were inserted in the corresponding well locations. Two log curves are required for the inversion i.e. P-wave log and density log. Normally, check-shot surveys are not acquired in each well in the field but it is better to use check-shot curves if available, because readings of check-shot surveys are acquired throughout the whole well unlike normal log curves. In this research project, check-shot survey of well 34/10-3 was primarily used which is shown in figure 4.1 below.

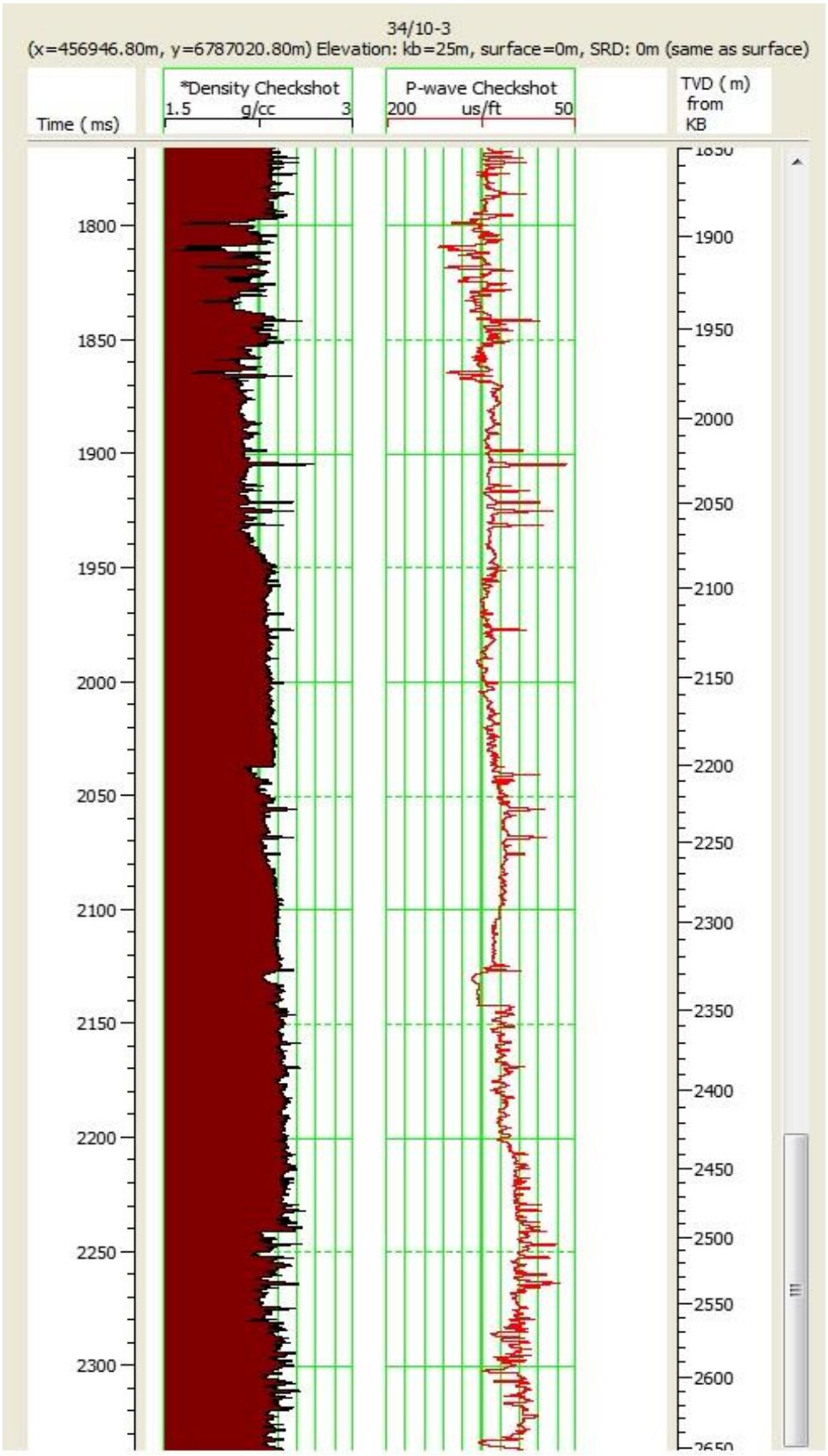

Figure 4.1: The check-shot survey (density and P-wave curve) from well 34/10-3 in reservoir zone.

Loading of the 3D seismic cube in the software is the next step of data loading process. After loading the 3D seismic cube, seismic view attributes can be changed such as vertical and horizontal scaling, colour combination etc. to view the structure more clearly on seismic section. The software displays selected well log curves on seismic section. An example of the inline 650 with P-wave curve from well 34/10-3 is shown in the figure 4.2.

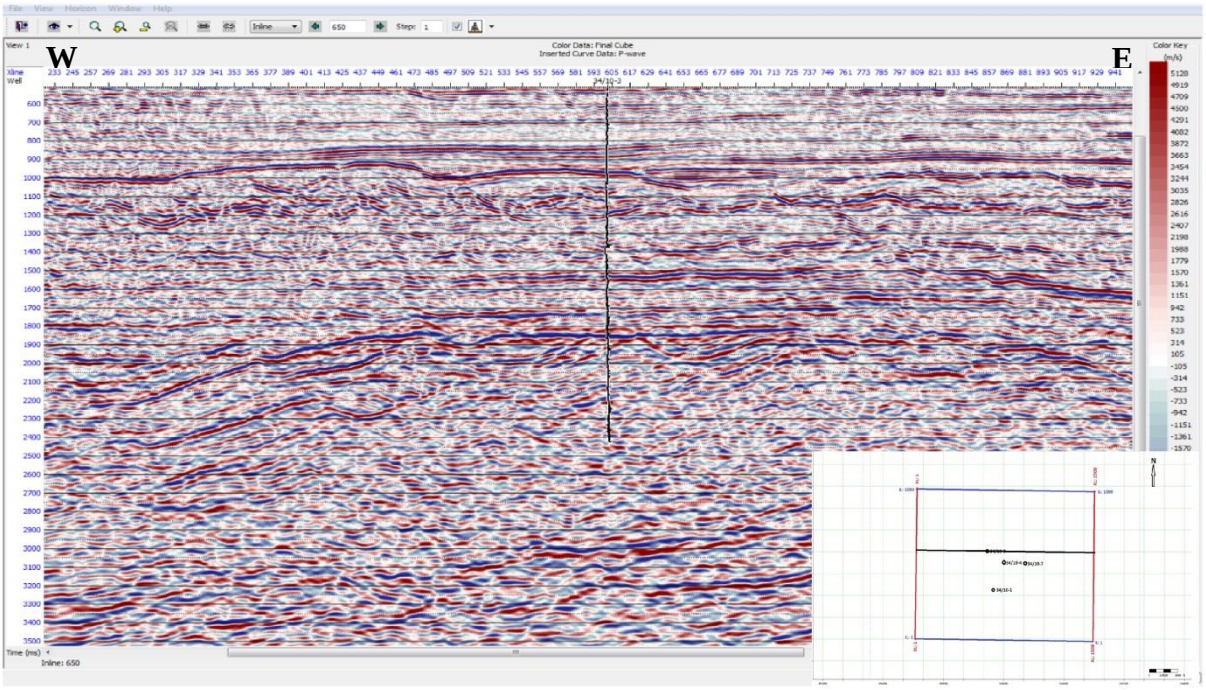

Figure 4.2: Figure showing inline 650 with P-wave curve from well 34/10-3. Red colour shows positive amplitudes whereas blue colour represents negative amplitudes.

An important component to build an initial model for inversion is to provide prior geological information such as reservoir geometry. This can be done by horizon and fault interpretation. Importing the already interpreted horizons can be done to the software if available. In the case of their unavailability, interpretation of the horizons is done by using either manual or automatic picking options in the software Strata. Manual picking should be a preferred option as auto-picking only follows higher or lower amplitudes which can lead us to incorrect results. Therefore, in this study, three horizons were interpreted on the basis of prominent amplitudes such as Top Brent, Drake formation and Statfjord formation. The information about the well tops was obtained from Norwegian Petroleum Directorate (NPD) website. Figure 4.3 shows the interpreted horizons.

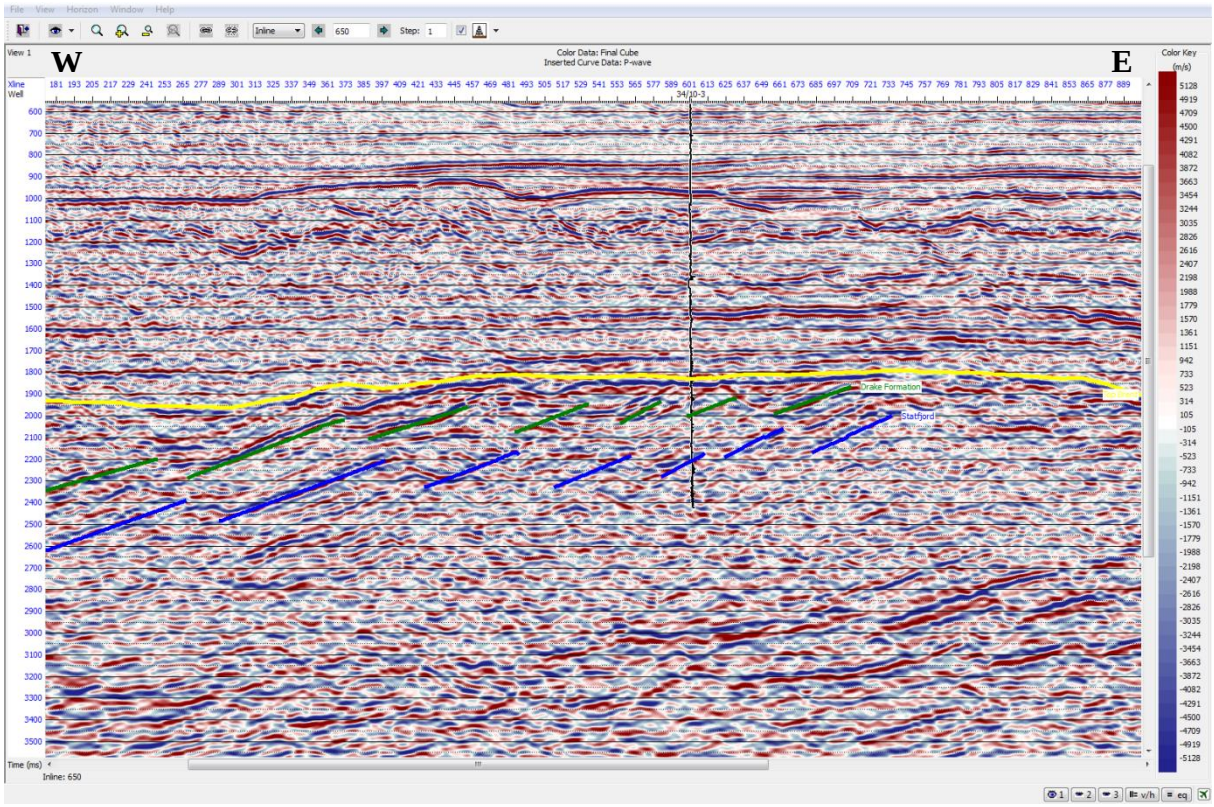

Figure 4.3: Figure showing horizon interpretation at inline 650. Yellow, green and blue colour represents Top Brent, Drake formation and Statfjord formation respectively.

4.2 Step 2: Well to Seismic Tie

The next step of seismic inversion process is to tie the wells with the real seismic data, in which events recorded on the well data are correlated with the events recorded on the seismic data. These events should be matched before proceeding to next step of seismic inversion.

Before proceeding towards well to seismic tie step, quality control of data was done especially in the case of well log data. Normally washouts and other bad borehole conditions affect the log readings which lead to wrong interpretation. To start a well to seismic tie a synthetic trace was created to correlate with the recorded seismic trace. The synthetic trace was generated from the well logs. In order to convert well logs from depth to two way travel time units and to generating synthetic seismic trace check-shot surveys were used. Hence density and P-wave logs values were combined to get the reflectivity spikes. Ideally this procedure should have been repeated with all the available wells in the area. But we have chosen logs from well 34/10-3 only. The reflectivity spikes log is stored in the software database and shown on the screen after convolving with a wavelet as a synthetic seismic trace. A suitable wavelet was estimated either from real seismic data or using well logs. The wavelet estimated from the real seismic, called *statistical wavelet*. This wavelet is a symmetrical as shown in the figure 4.4 given below.

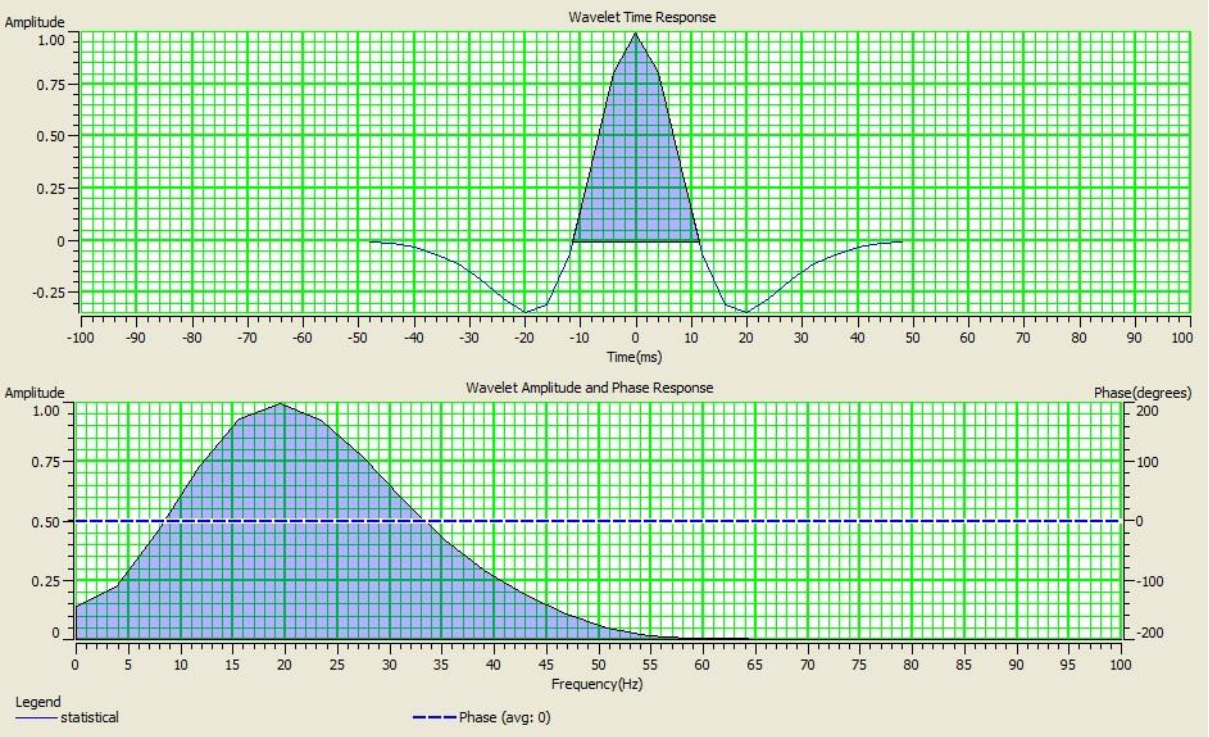

Figure 4.4: Showing the statistical wavelet with amplitude/time graph the upper half and amplitude/frequency graph in the lower half.

And the wavelet extracted from the wells logs is called *wavelet using wells*. This wavelet is non-symmetrical and is phase shifted comparatively to the statistical wavelet. The figure 4.5 shows the wavelet estimated from the wells 34/10-1, 34/10- 3, 34/10-4 and 34/10-7.

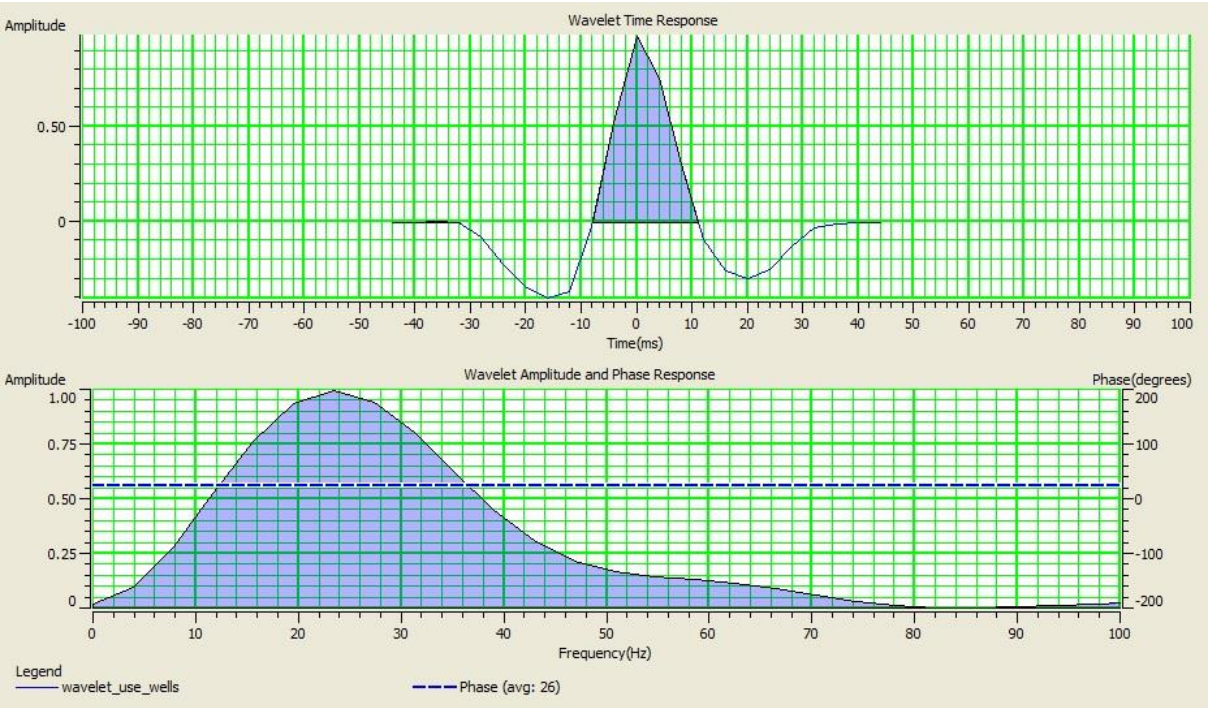

Figure 4.4: Figure showing the wavelet using wells with amplitude/time graph in the upper half and amplitude/frequency graph in the lower half.

The difference between the two extracted wavelets is shown in the figure below. The black shaded wavelet is the statistical wavelet whereas wavelet extracted from wells is shown in blue colour.

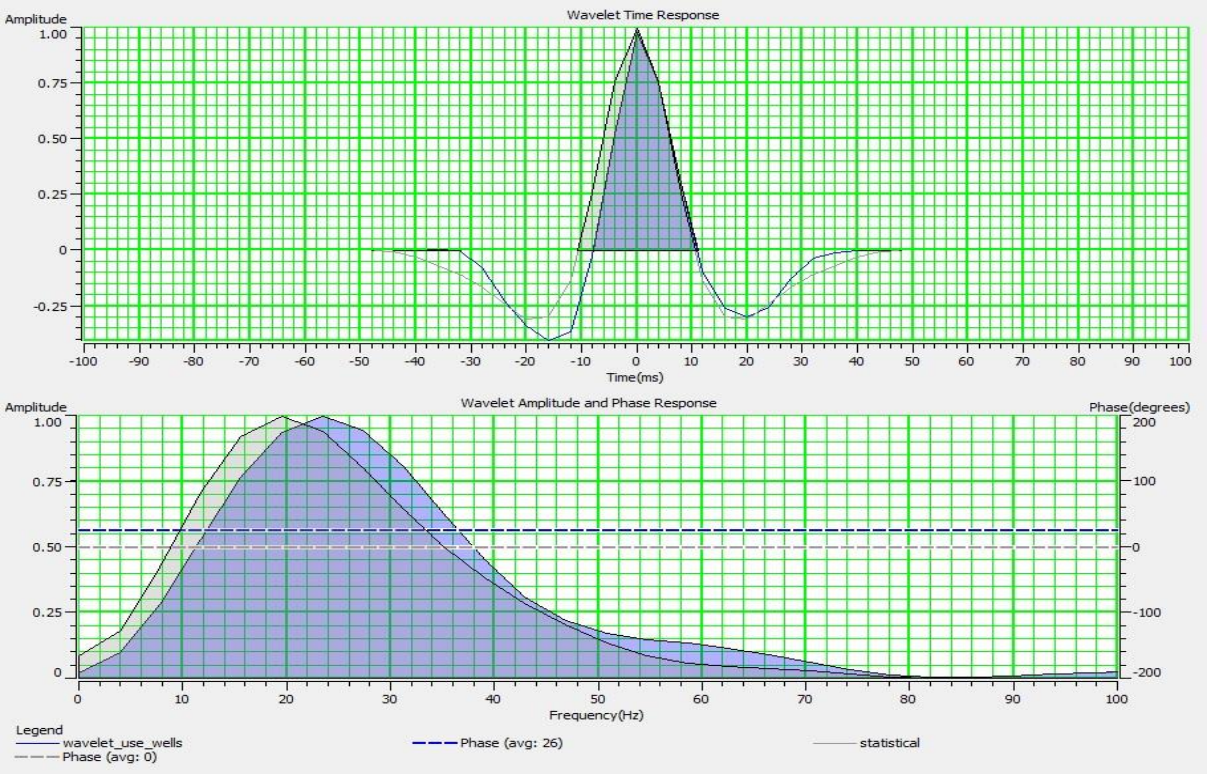

Figure 4.6: Figure showing the difference between statistical and wavelet extracted from wells.

The estimated wavelets were then convolved with the reflectivity spikes one by one to get a synthetic trace. The obtained blue synthetic trace was then correlated with the red composite trace, which is the average of real seismic traces around the well bore. The synthetic trace using statistical wavelet is correlated first. The figure 4.7 shows synthetic trace constructed from well 34/10-3 was correlated with the real seismic data.

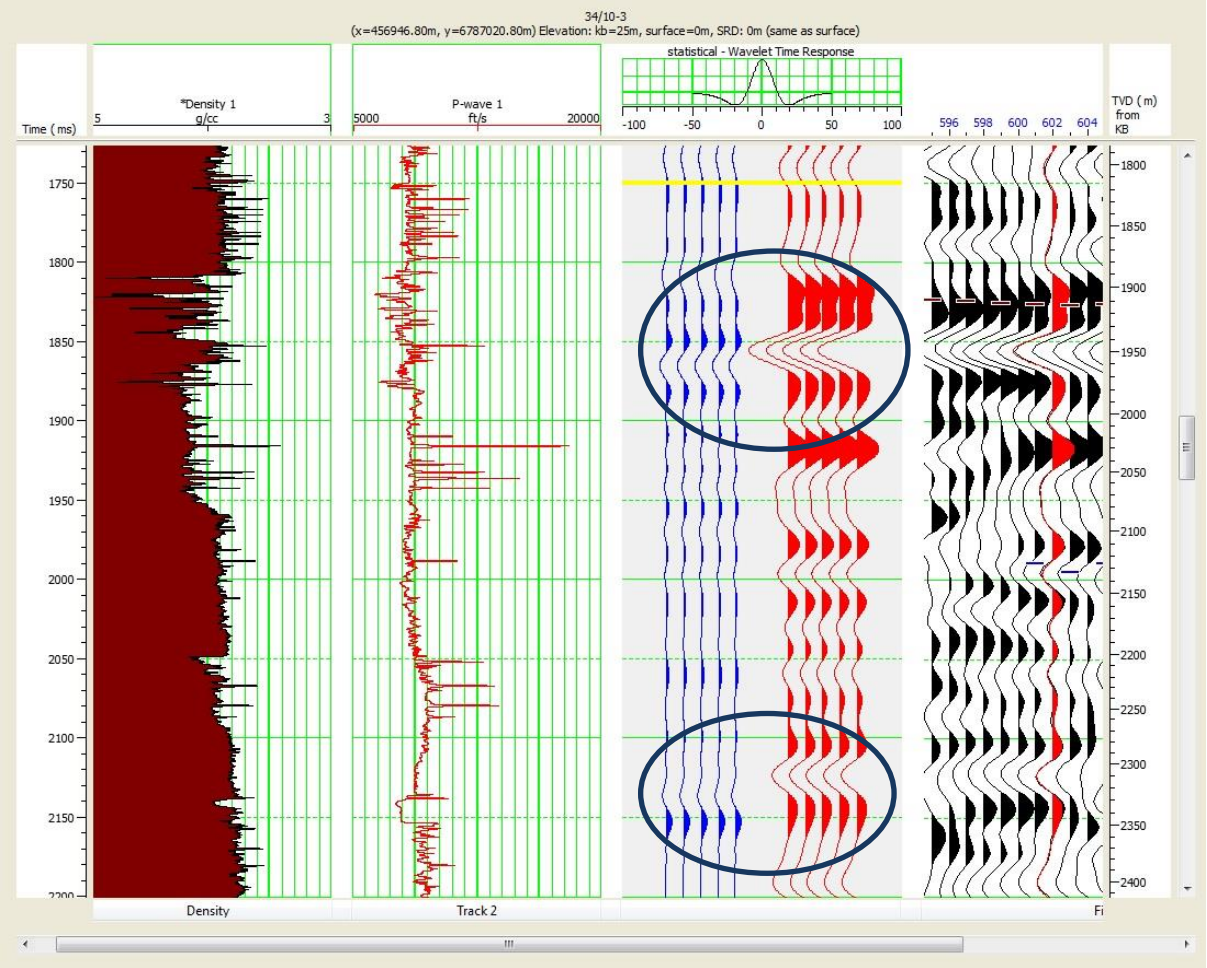

Figure 4.7: Figure showing correlation of blue synthetic trace with the red composite trace from real seismic data.

In the figure 4.7 shows the events which are not matching, highlighted in the circles. The correlation coefficient value in this case is very small i.e. 0.37 and lag of time shown in figure 4.8. The value was improved by the suggested shifting up of the synthetic traces by the software. The suggested shifting value by the Strata depends upon the selected correlation window, which means bigger the correlation window, higher the miss match and vice versa. As our target zone is the reservoir zone, therefore correlation window of target zone was selected only. Even after applying suggested 17 ms of shift there was still a small time lag between synthetic and real seismic trace.

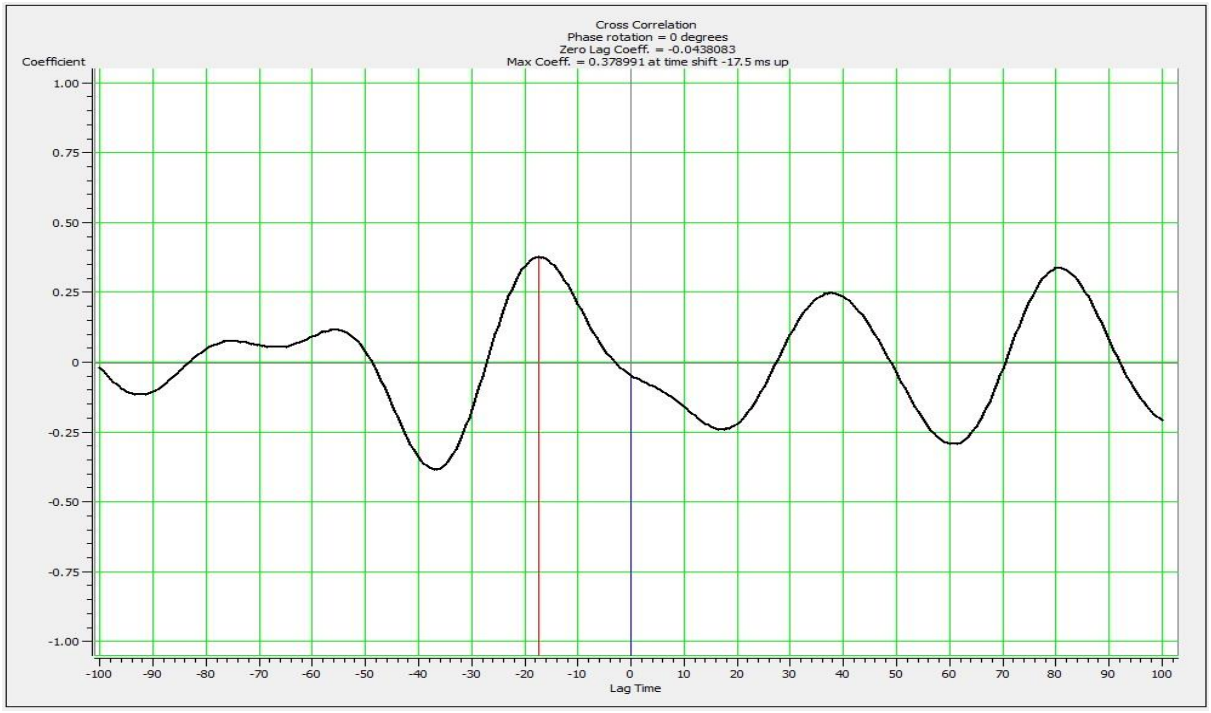

Figure 4.8: of suggested shift of statistical wavelet

Therefore new synthetic trace was computed using wavelet extracted from the wells and correlated with the red composite trace. It was observed that the Strata suggested 0.5 ms of upward shift of synthetic trace shown in the figure 4.9 below.

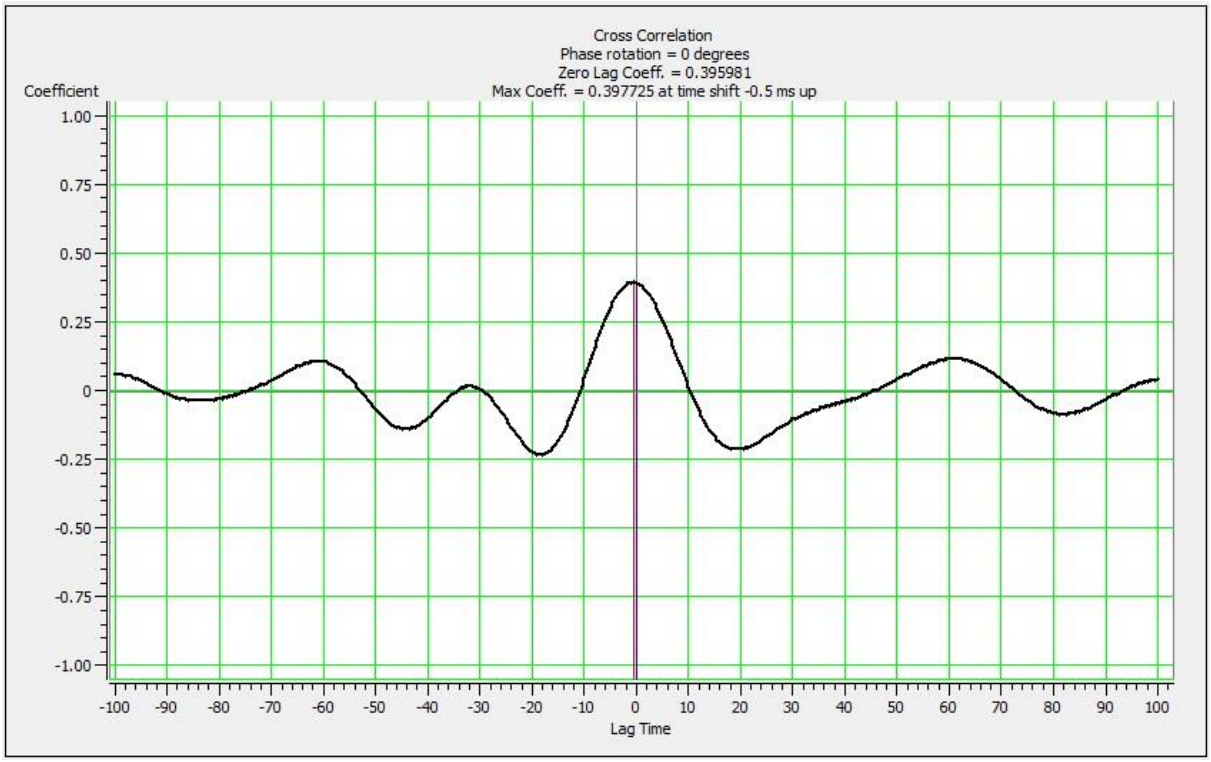

Figure 4.9: Graph showing time lag of the synthetic trace represented by blue line, overlying with minute difference of red line of composite trace.

After applying the suggested shift of synthetic trace, we get the best fit match with the composite trace in the reservoir zone as shown in the figure 4.10.

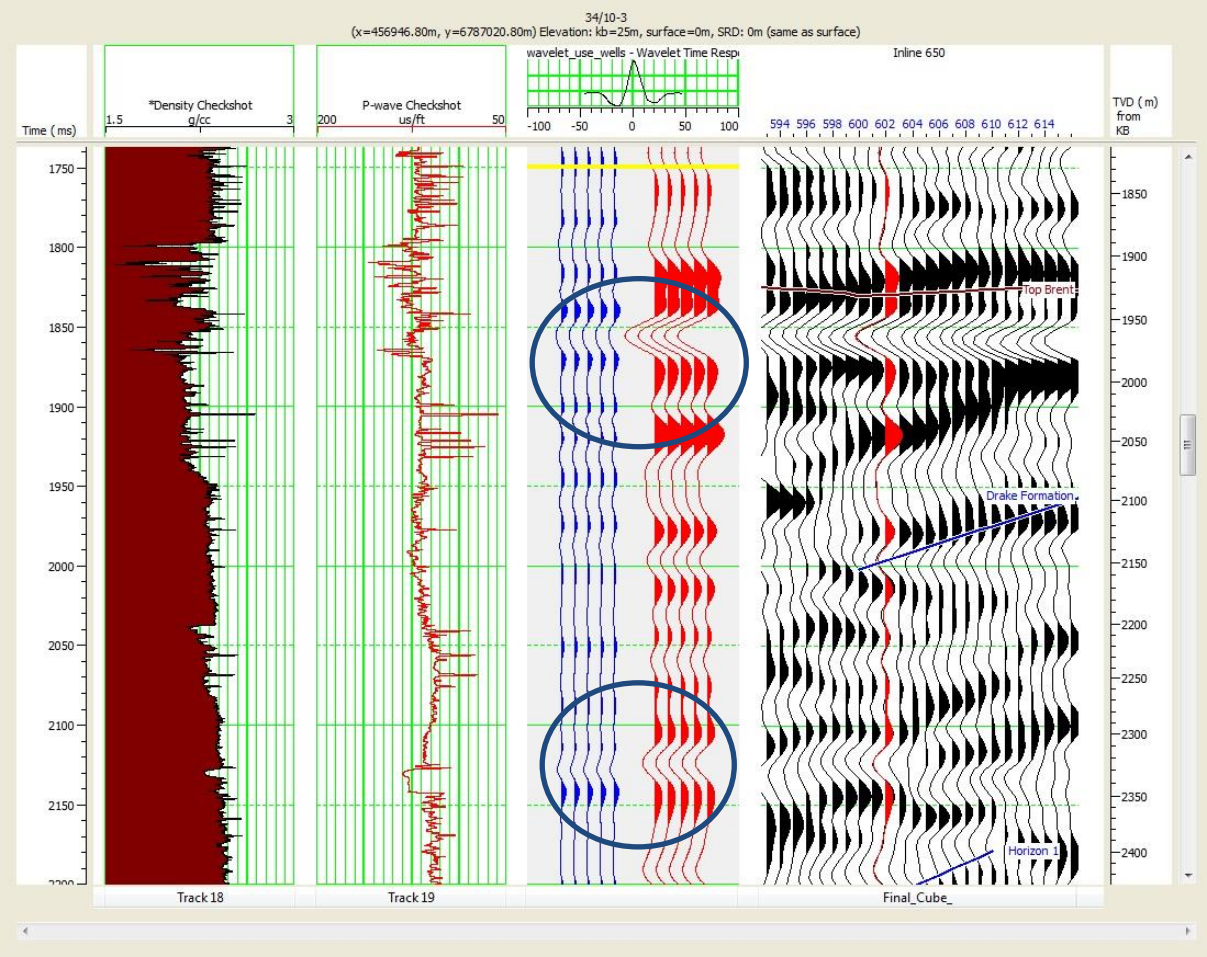

Figure 4.10: Figure showing best fit match of the blue synthetic trace with the red composite trace.

In the figure 4.10, the events highlighted in the circles are well correlated now. On the basis of correlation, the Strata computed a new log called P-wave corrected log which was used in building of the initial model.

4.3 Step 3: Initial Model

The next step is the initial model building. In the current research project, two initial models were built. First model was the acoustic impedance model computed from P-wave impedance log and the other was elastic impedance model at 0 degree angle computed from S-wave impedance log respectively. The figure 5.1 and figure 5.2 shows acoustic impedance and elastic impedance initial models, respectively. There are number of parameters which needed to be set before building the initial model. These parameters included horizons to be displayed in the model, wells to be included, selecting the computed impedance logs used for making model, trace filtering options: These initial models were used for different inversion techniques to be analysed.

4.4 Step 4: Inversion Techniques Applied

After building initial model, different inversion techniques were applied on it and inversion analysis was done. Four different inversion techniques, using both the initial models, were applied i.e. Model Based, Bandlimited, Sparse Spike and coloured inversion. In the beginning inversion techniques were only applied to one seismic line i.e. inline 650 with well 34/10-3. For the Model Based and Sparse Spike techniques different parameters were set to obtain the results. These parameters included maximum impedance change for upper and lower value and inversion trace scalar options. The results are shown in the chapter 5.. The results obtained by using two different initial models were compared with each other and analysed.

Chapter 5: Results and Discussion

5.1 Initial Model

The figure 5.1 and 5.2 shows the initial acoustic and elastic impedance models using inline 650 with inserted P-wave curve from well 34/10-3. In these models, colour variation shows change in colour amplitudes that corresponds to the acoustic impedances and elastic impedances.

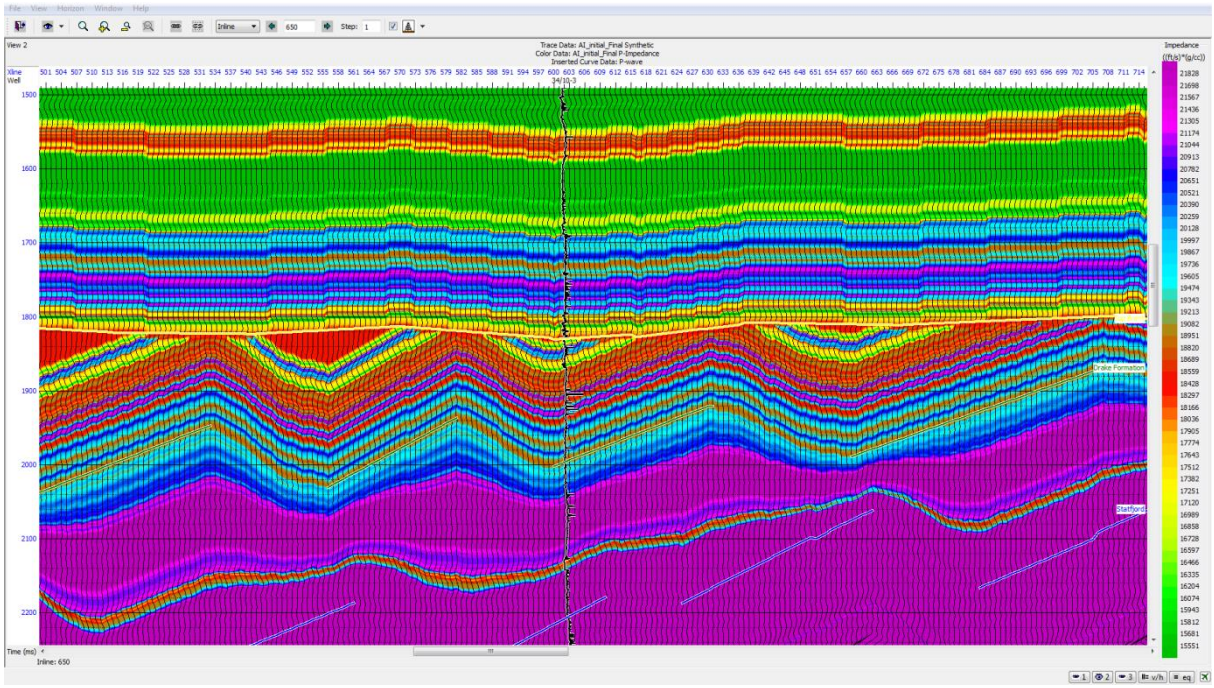

Figure 5.1: Initial acoustic impedance model with P-wave inserted.

The bright colours in the figure 5.1 show high amplitudes whereas light colours show low amplitudes. The trace data in the both models shown in the figure 5.1 and 5.2 is the synthetic traces computed during well correlation.

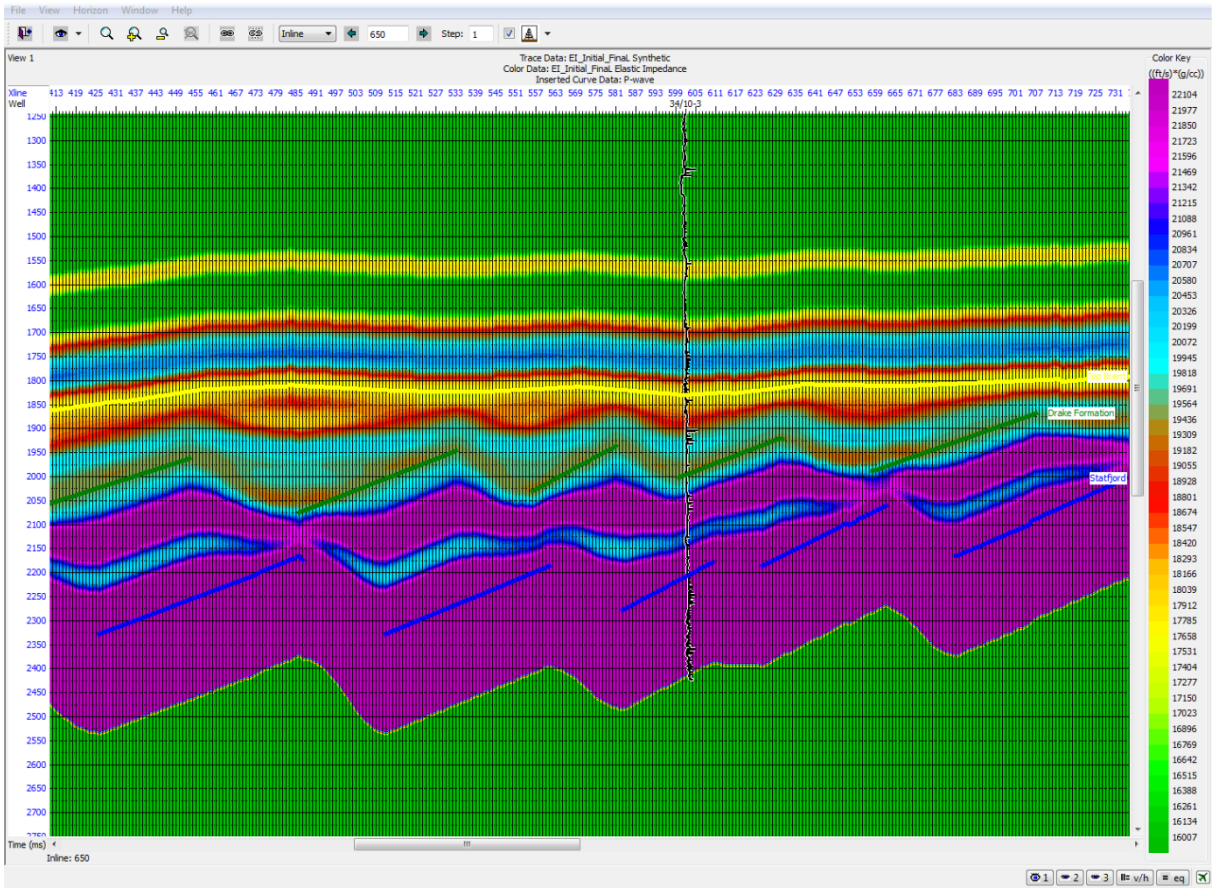

Figure 5.2: Initial elastic impedance model P-wave log inserted.

While building the initial elastic impedance model, offset/angle specification was set at zero. In principle, the model should show similar results as acoustic impedance model, but the obtained results, however, show some difference as shown in figure 5.3. A comparison between the two initial models is given in the figure below 5.3. The elastic impedance model is shown at left hand side whereas acoustic impedance model is shown at right hand side. The difference is clearly visible as the colour variation is less in elastic impedance model than acoustic impedance model. The acoustic impedance model is a high frequency model as compared to the elastic impedance model marked by black circles in the figure 5.3.

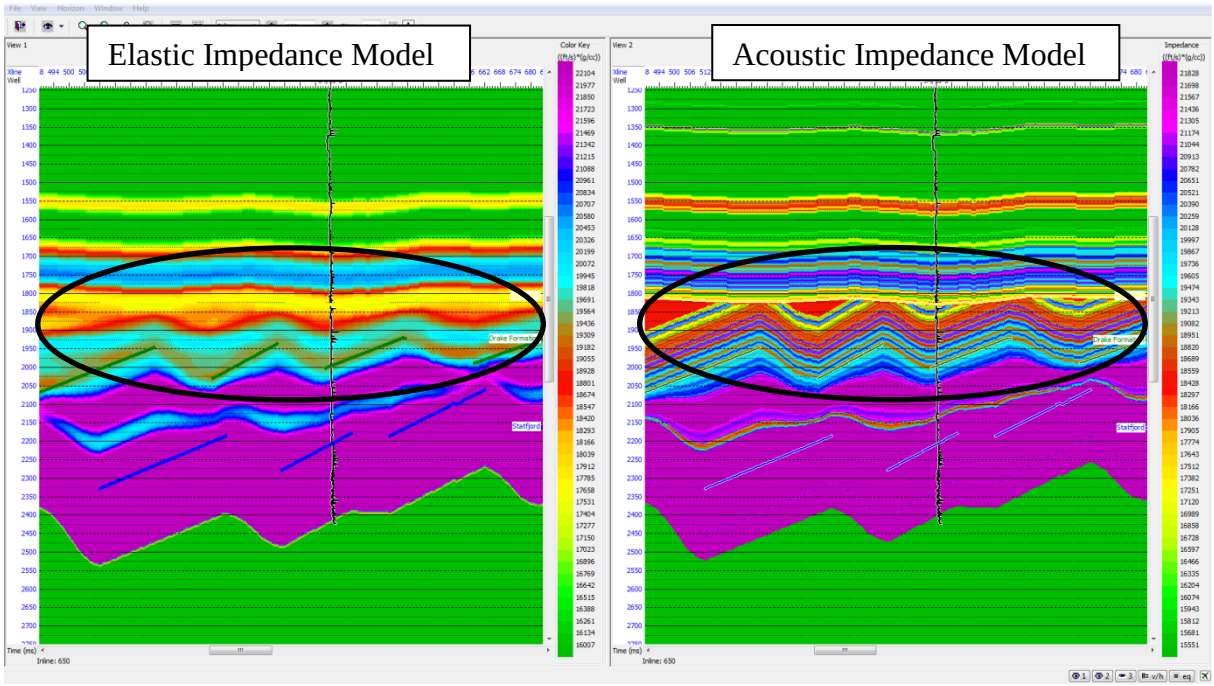

Figure 5.3: Elastic impedance model (left), acoustic impedance model (right).

5.2 Inversion Analysis

For the inversion analysis, four different inversion techniques were applied on both the initial impedance models. They are listed as follows

1. Model Based
2. Bandlimited
3. Linear Programming Sparse Spike
4. Maximum Likelihood Sparse Spike

All of these inversion techniques were first applied to initial acoustic impedance model and later to the initial elastic impedance. The results of these inversion techniques are presented from figures 5.4 to figure 5.15. The wavelet extracted from wells was used for all the inversion analysis. The inversion analysis is done only for the reservoir zone i.e. from 1700 ms to 2400 ms at time section.

5.2.1 Model Based Inversion

The figure 5.4 and figure 5.5 shows the result of Model Based inversion applied on acoustic and elastic impedance models, respectively.

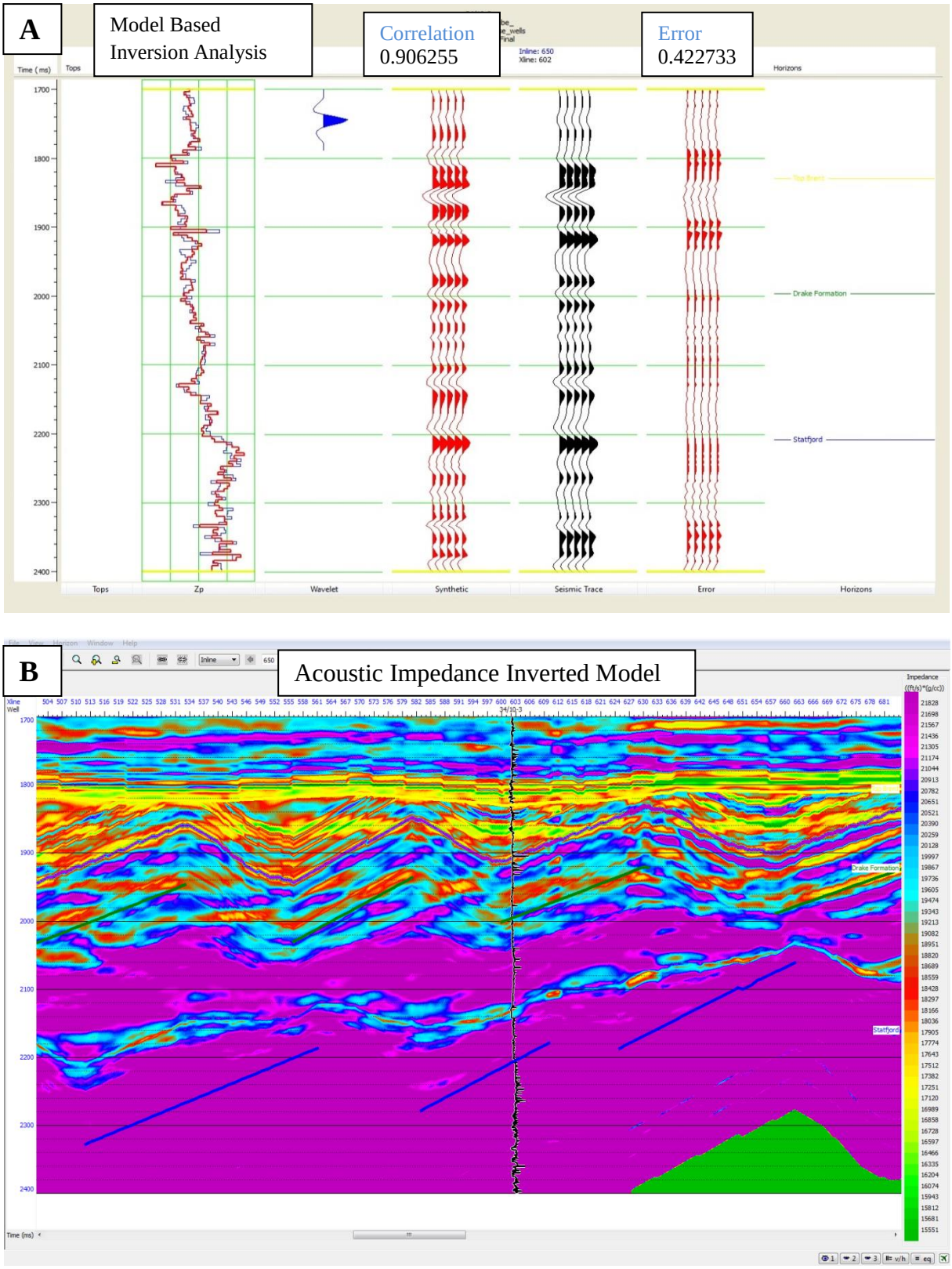

Figure 5.4: Model Based inversion analysis using acoustic initial impedance model is shown in A and inverted model is shown in B. The black traces in A correspond to the actual seismic traces whereas red traces as synthetic seismic traces.

The figure 5.4 gives us Model Based inversion analysis in A, in which error is 0.422, giving a very good correlation of 0.906. The black traces in the analysis represent the actual seismic

traces whereas red traces are the synthetic traces. Similarly, the figure 5.5 below shows the Model based inversion analysis of elastic impedance model with error of 0.344 giving correlation of 0.941.

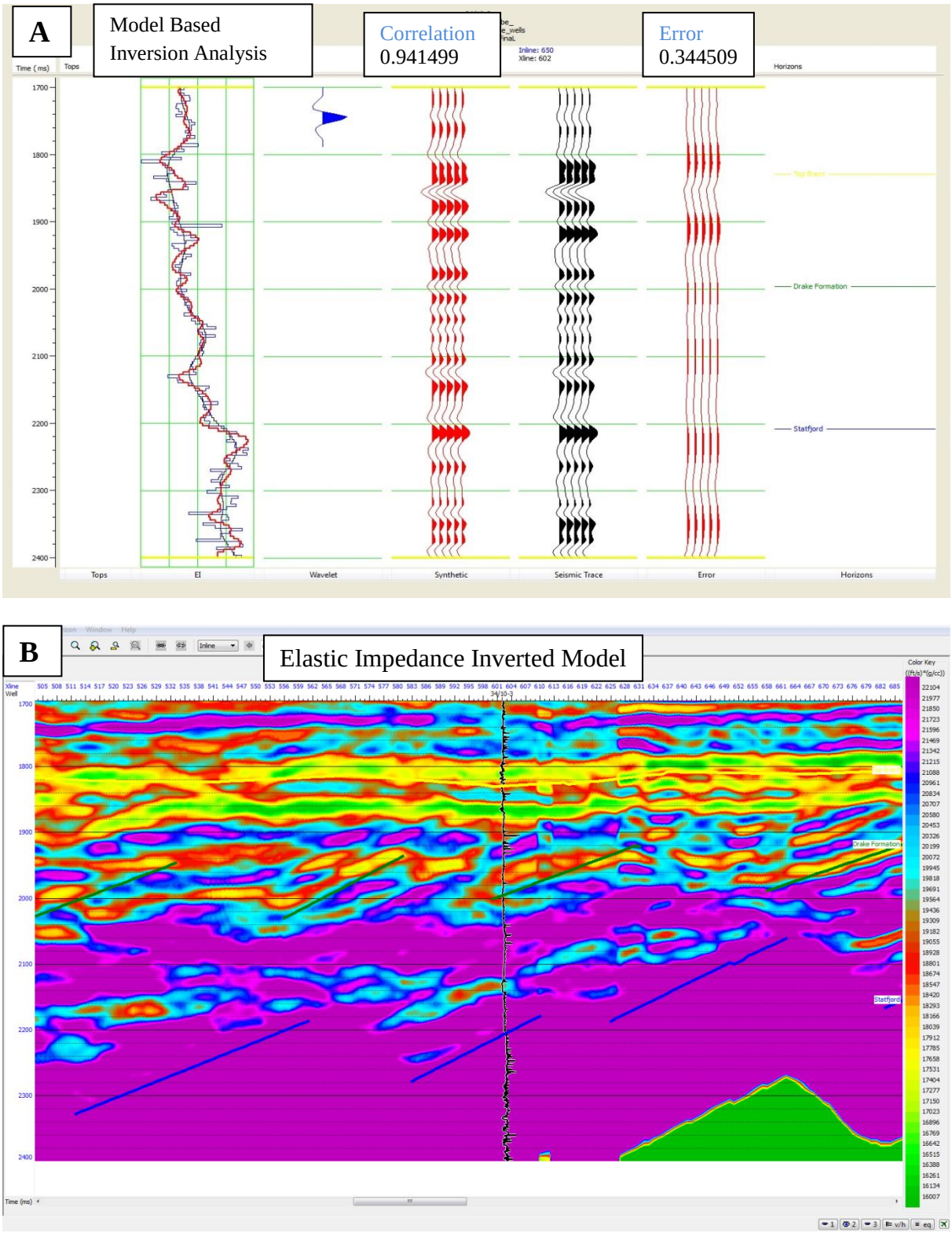

Figure 5.5: Model Based inversion analysis using elastic initial impedance model is shown in A and inverted model is shown in B. The black traces in A correspond to the actual seismic traces whereas red traces as synthetic seismic traces.

A comparison has been made between the inversion results of the two different initial models. The figure 5.6 shows inversion results of acoustic impedance initial model on left hand side whereas inversion results from elastic impedance model on right hand side.

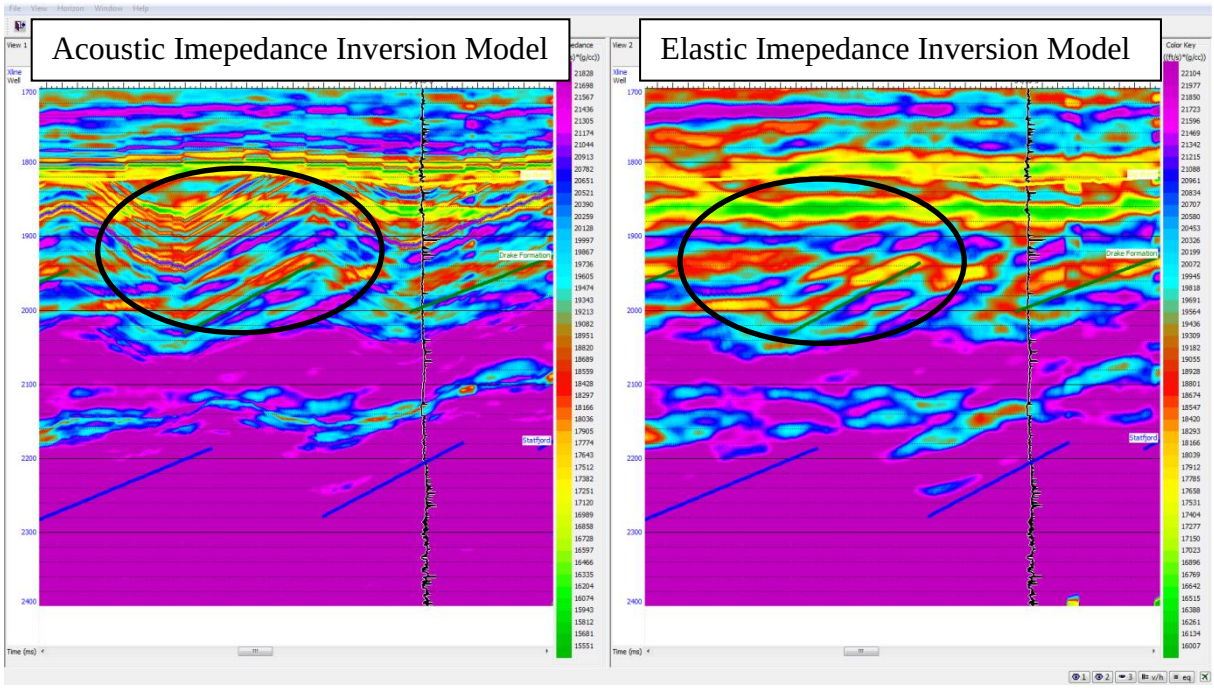

Figure 2.6: The two Model based inversion results using acoustic and elastic initial impedance model.

It is clear from the results that acoustic impedance initial model gives better results. The coloured amplitudes are better distinguishable that corresponds to the acoustic impedance contrast, highlighted in black circles in the figure 5.6. The acoustic impedance initial model gives better lithological information as well such as dipping direction of the formations.

5.2.2 Bandlimited Inversion Analysis

The Bandlimited inversion analysis and results of both initial models are shown in the figure 5.7 and figure 5.8.

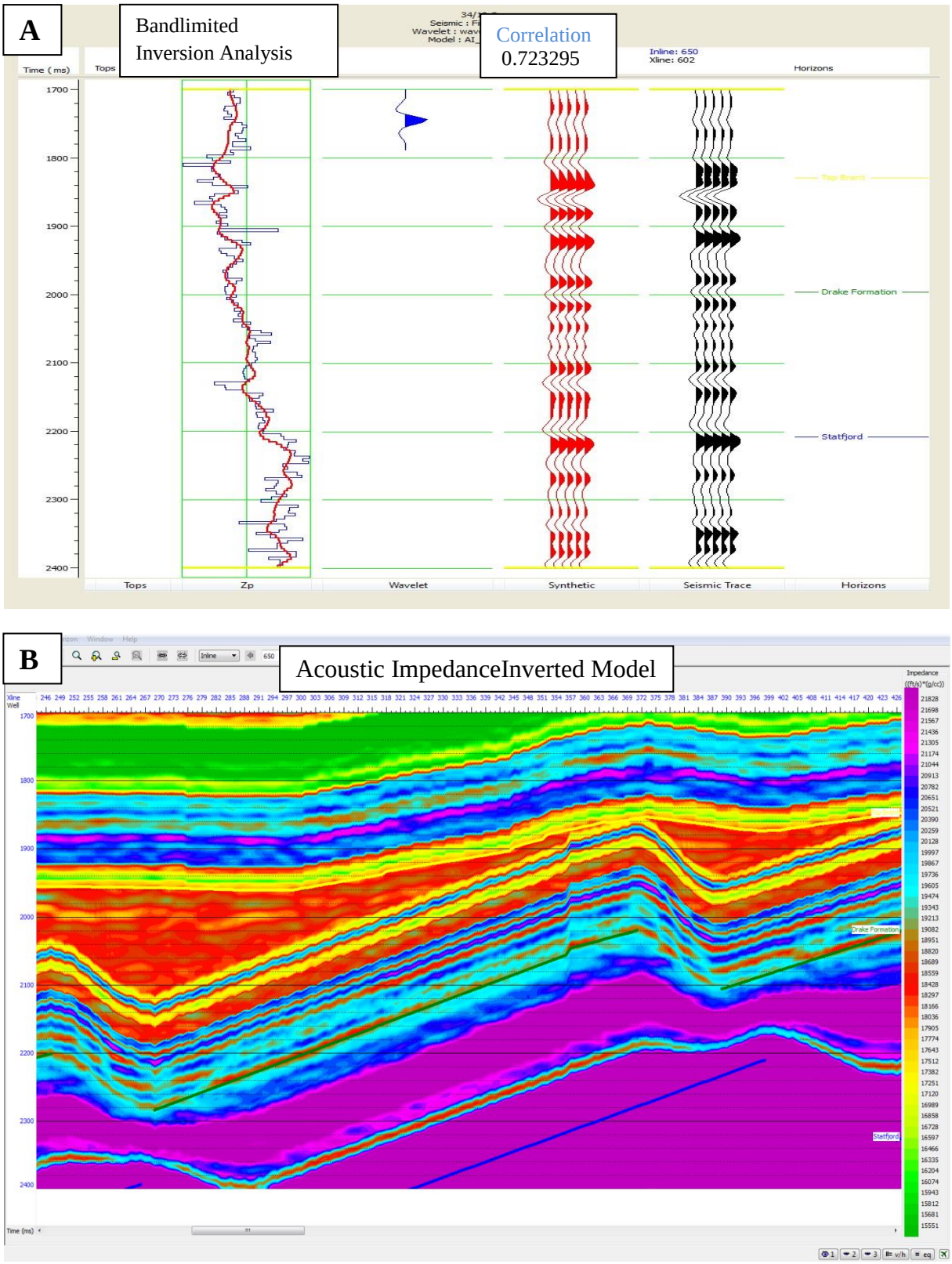

Figure 5.7: Bandlimited inversion analysis using acoustic initial impedance model is shown in A and inverted model is shown in B. The black traces in A correspond to the actual seismic traces whereas red traces as synthetic seismic traces.

The Bandlimited inversion analysis gave the correlation of 0.72. The inversion parameter such as constrain high-cut frequency is set at 10Hz used for this model. The Bandlimited

inversion analysis on the elastic impedance model shows a correlation of 0.74 given in the figure 5.8.

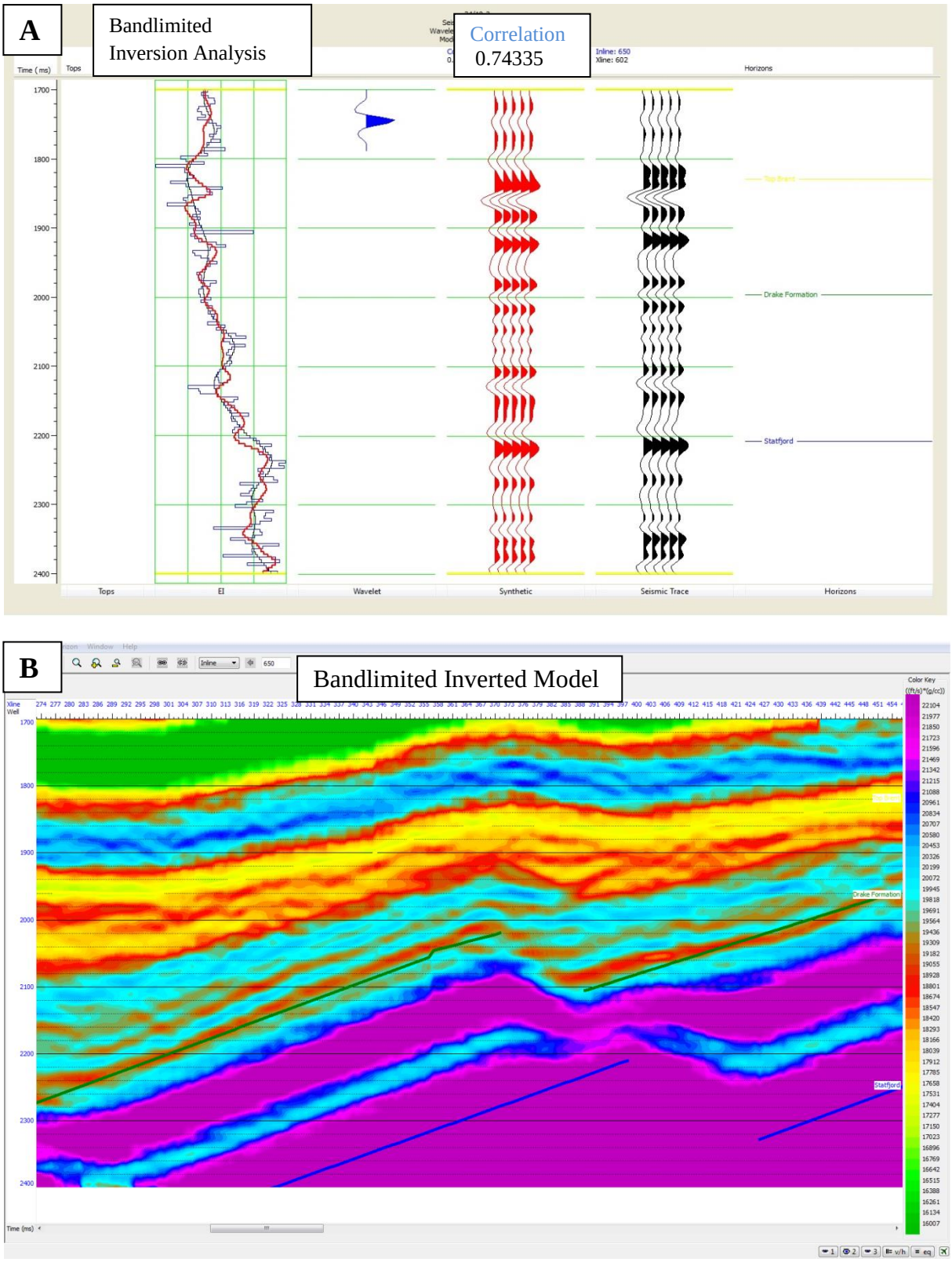

Figure 5.8: Bandlimited inversion analysis using elastic initial impedance model is shown in A and inverted model is shown in B. The black traces in A correspond to the actual seismic traces whereas red traces as synthetic seismic traces.

By comparing the results of both the inverted models a clear difference in the reservoir zone has been observed, which is marked in black circles. In the acoustic impedance inverted model the impedance contrast is sharp as compared to the elastic impedance inverted model.

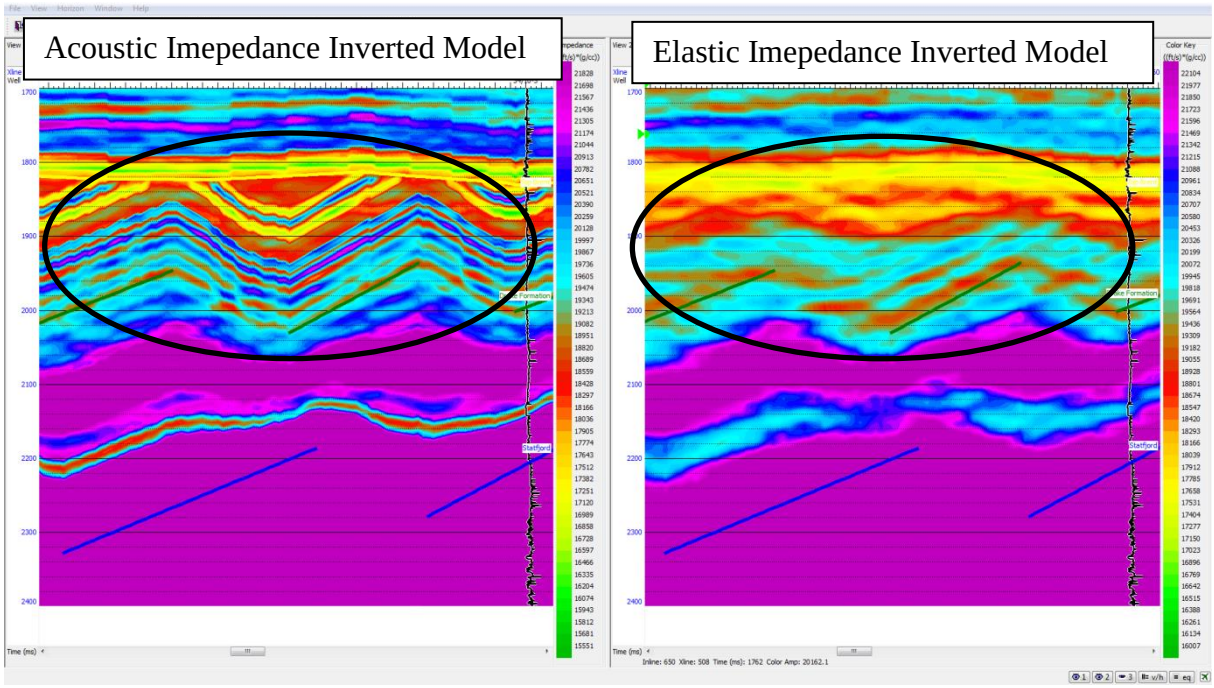

Figure 5.9: The two Bandlimited inverted models using acoustic and elastic initial impedance model.

5.2.3 Linear Programing Sparse Spike Inversion

The inversion analysis and inverted model of acoustic and elastic impedances models as a result of linear programing sparse spike inversion is given in the figures 5.10 and 5.11, respectively.

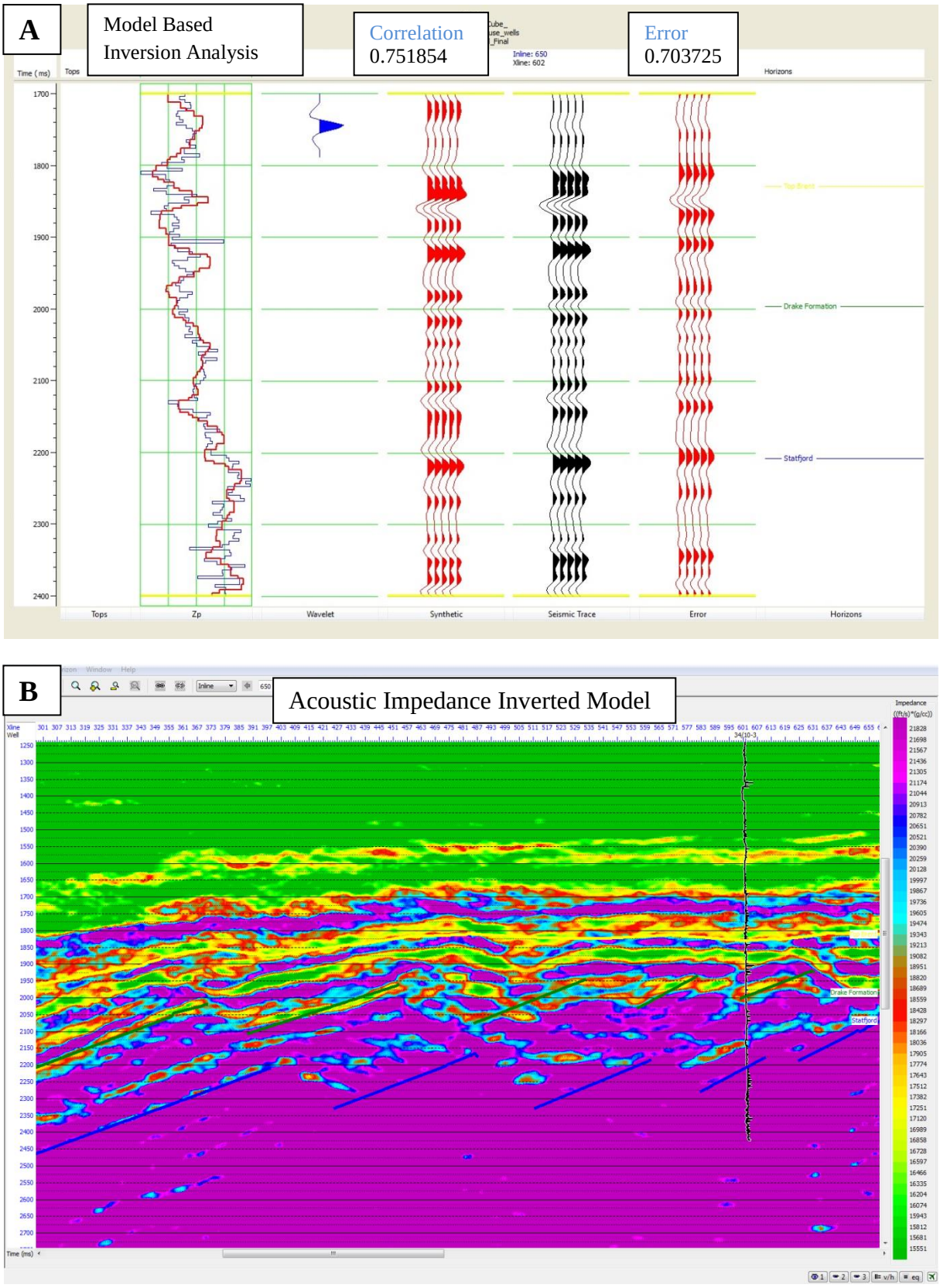

Figure 510: Linear Programing Sparse Spike inversion analysis using acoustic initial impedance model is shown in A and inverted model is shown in B. The black traces in A correspond to the actual seismic traces whereas red traces as synthetic seismic traces.

In the Linear Programing Sparse Spike inversion analysis using acoustic impedance initial model, the error increases up to 0.70 and correlation decreases to 0.75, which gives bad results. Interpretation of inverted model became quite difficult as the colours in the model changes abruptly. Similarly, with the same error and correlation, elastic impedance inverted model gives less clear results as shown in the figure 5.11.

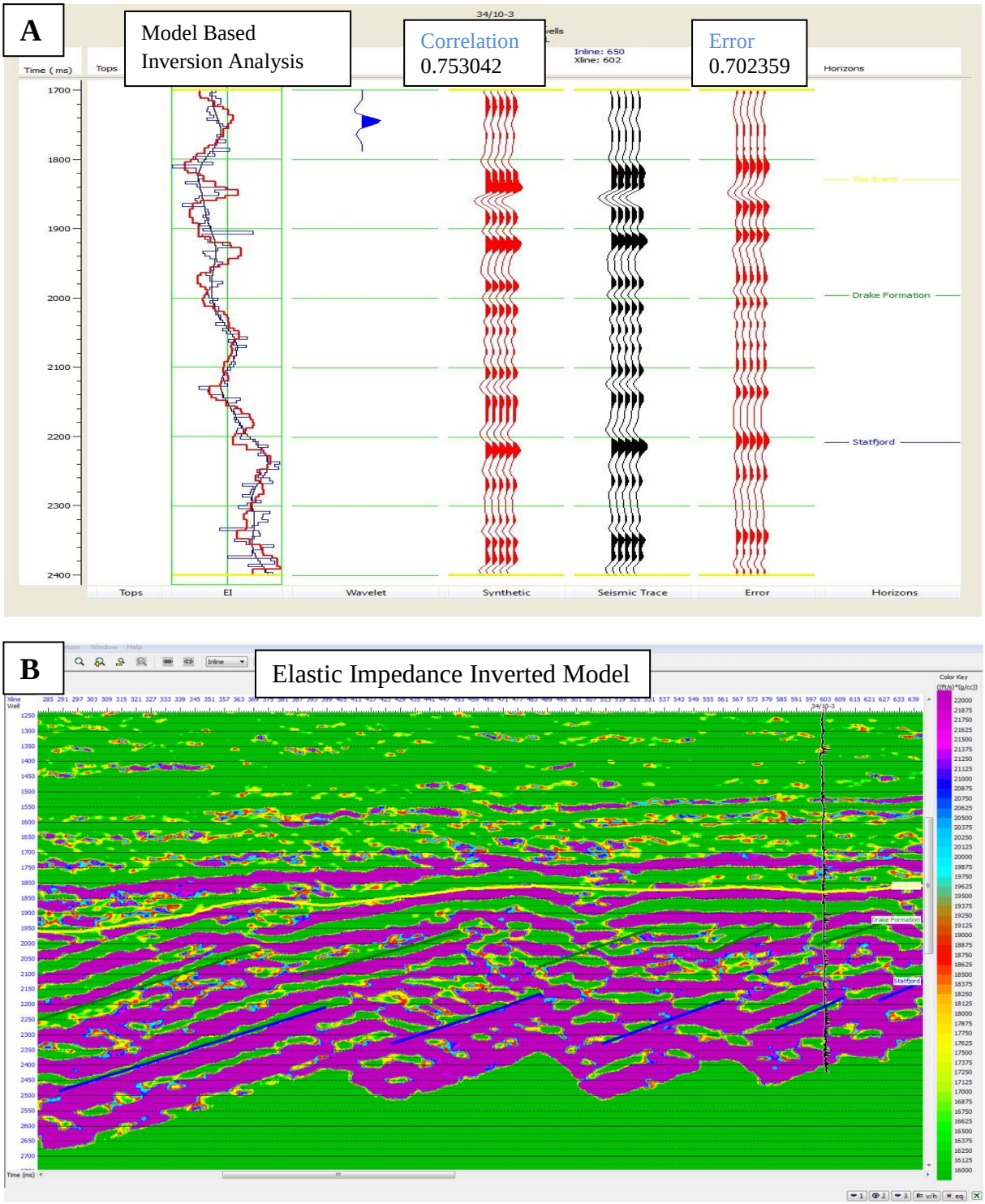

Figure 5.11: Linear Programing Sparse Spike analysis using elastic initial impedance model is shown in A and inverted model is shown in B. The black traces in A correspond to the actual seismic traces whereas red traces as synthetic seismic traces.

If we compare results of both the inverted models, the acoustic impedance inverted model gives slightly better results than elastic impedance inverted model shown in figure below.

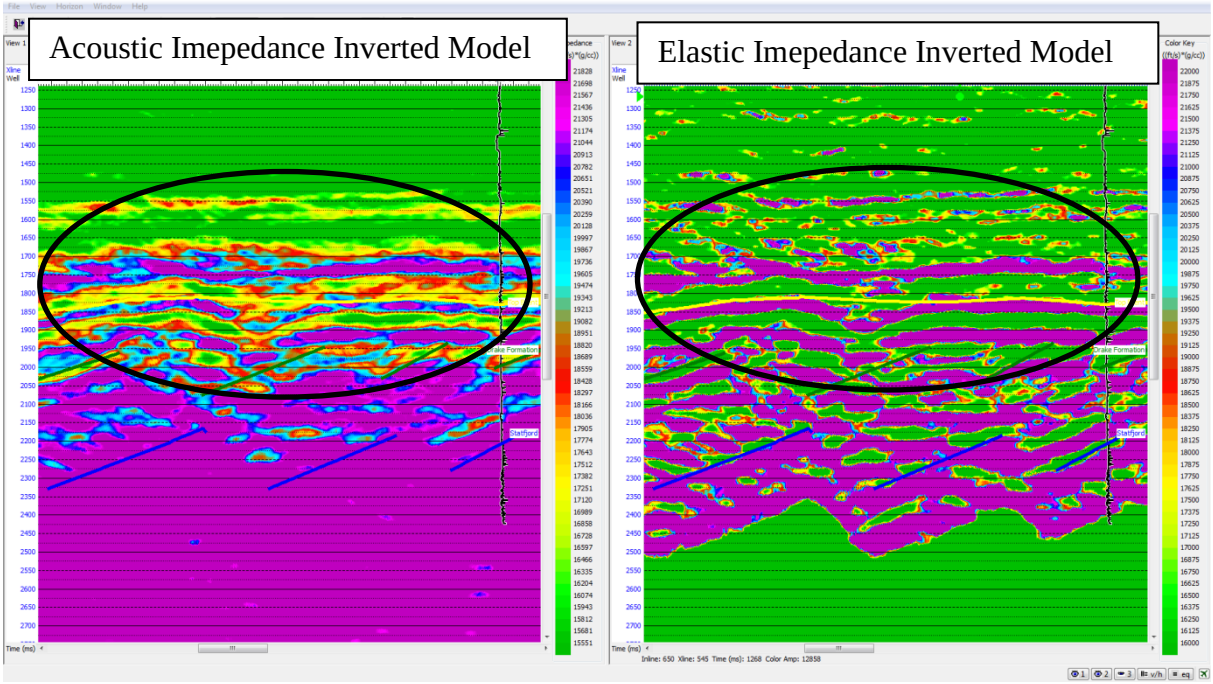

Figure 5.12: The two Linear Programing Sparse Spike inverted models using acoustic and elastic initial impedance model.

5.2.4 Maximum Likelihood Sparse Spike Inversion

The inverted models of the acoustic and elastic impedances models using Maximum Likelihood Sparse Spike inversion are given in the figure 5.13 and 5.14.

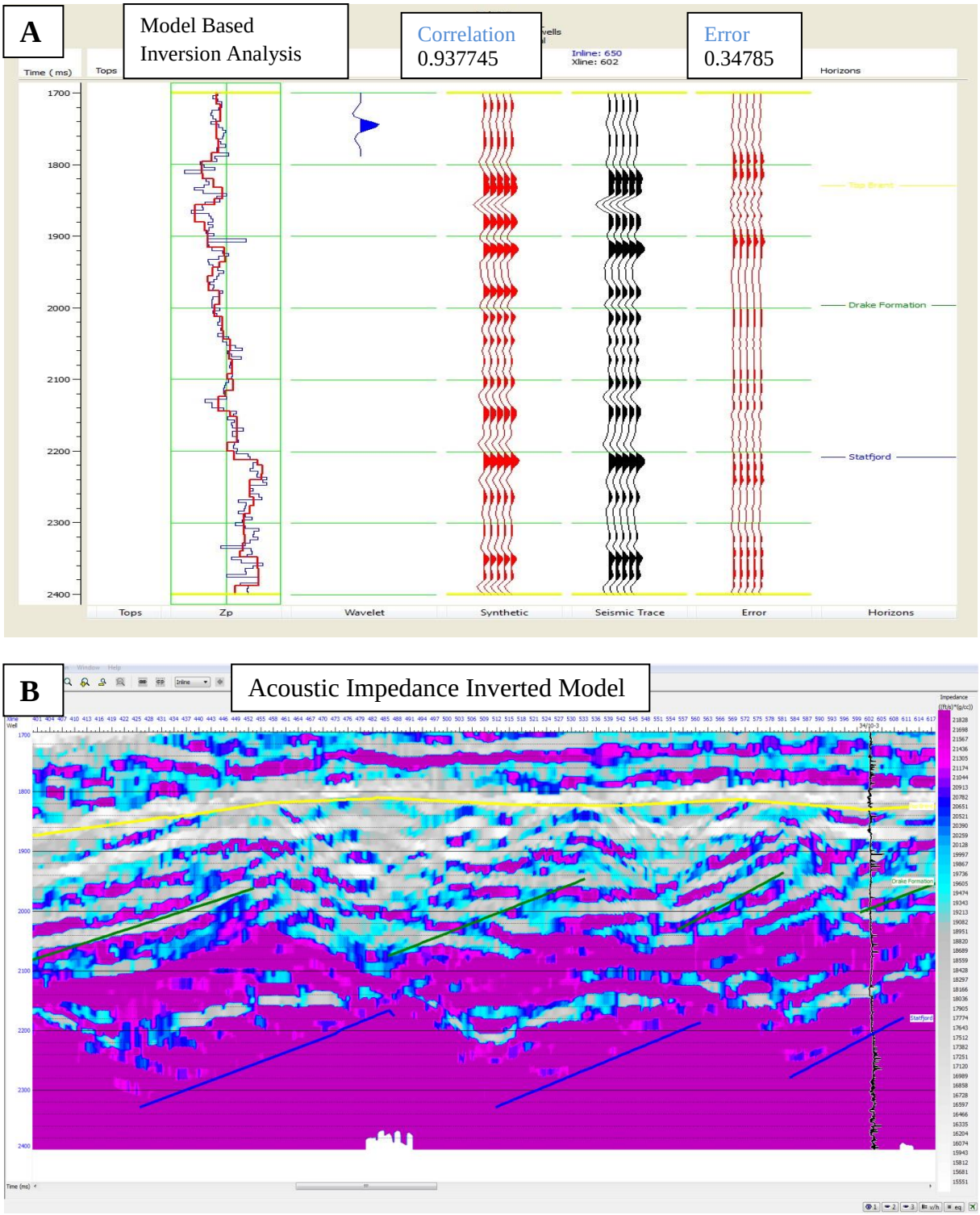

Figure 5.13: Showing Maximum Likelihood Sparse analysis using acoustic initial impedance model is shown in A and inverted model is shown in B. The black traces in A correspond to the actual seismic traces whereas red traces as synthetic seismic traces.

The inversion analysis in the figure 5.13 shows good correlation of 0.937 with the error of 0.35. But the error increases in elastic impedance model up to 0.416 giving correlation of 0.91, which is still not a bad correlation. The figure 5.14 shows the inversion analysis and inverted model of the elastic impedance initial model.

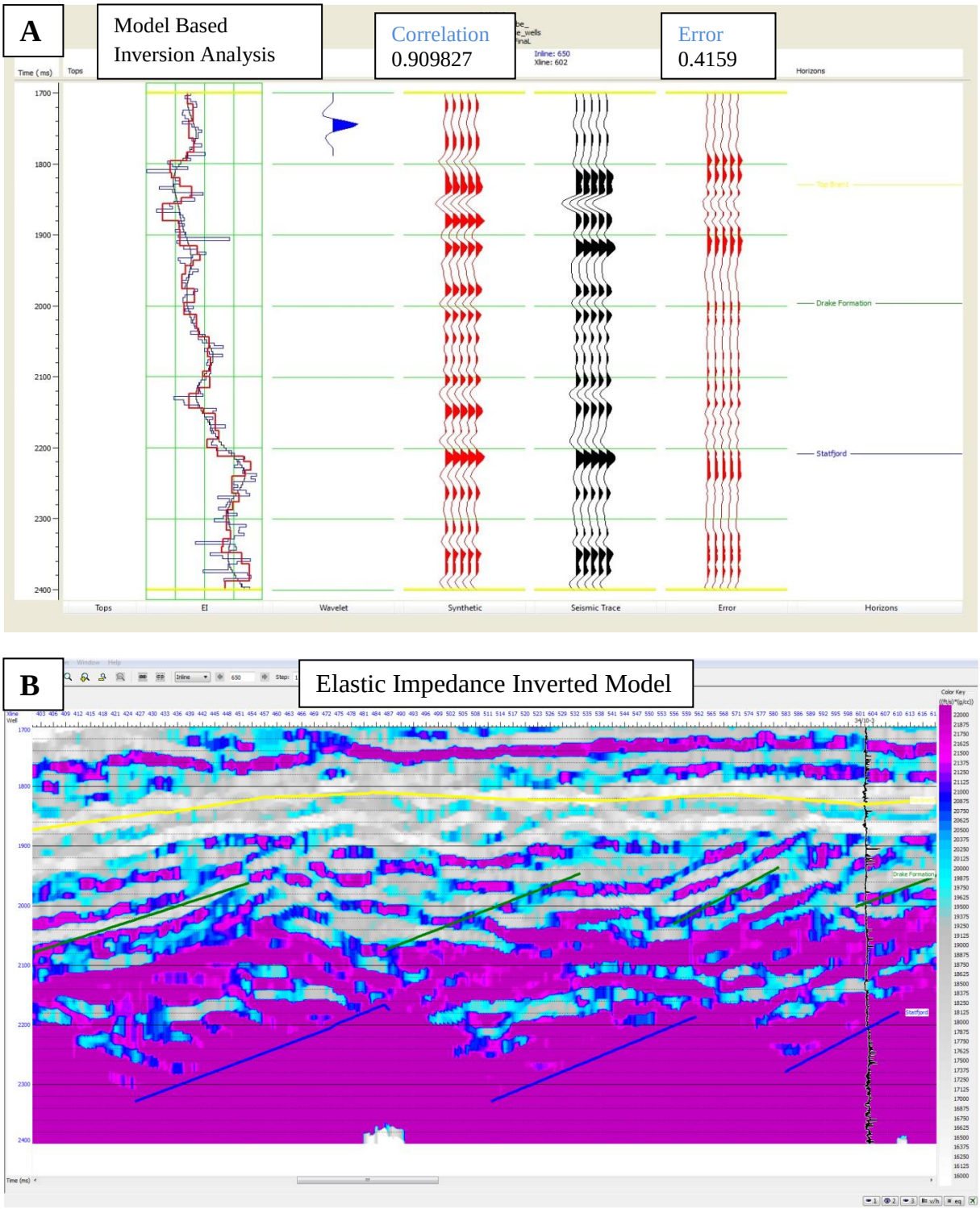

Figure 5.14: Showing Maximum Likelihood Sparse Spike analysis using elastic initial impedance model is shown in A and inverted model is shown in B. The black traces in A correspond to the actual seismic traces whereas red traces as synthetic seismic traces.

If we compare the inverted models of acoustic and elastic initial impedance models with each other, the results are not very different and more or less same as shown in the figure below.

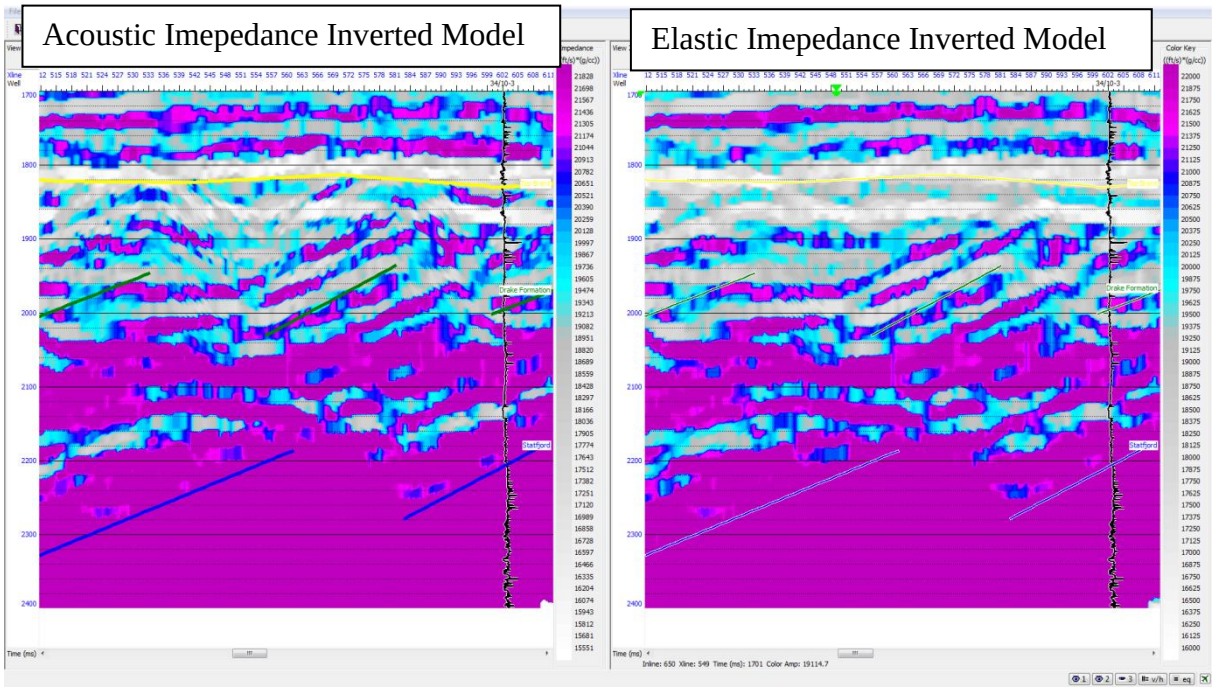

Figure 5.15: The two Linear Programing Sparse Spike inverted models using acoustic and elastic initial impedance model.

During well to seismic tie, zero phase (statistical) wavelet was used initially, but a small miss match retained between synthetic seismic trace and true seismic trace. The miss match was removed by using minimum phase wavelet, extracted from all the available well data to get the best fit match. As per usual practice, acoustic impedance initial model was built using full-stack seismic data, but elastic impedance initial model was also build using the same seismic data and keeping the offset zero. Theoretically, there should be no difference between both the initial impedance models but practically, the results were found considerably different as shown in the figure 5.3.

Different inversion algorithms were applied to the initial impedance models and their results were compared. There was notable difference found in the inverted models of the acoustic and elastic initial impedance models. Due to certain limitations such as unavailability of pre-stack seismic data, it is difficult to reach the conclusion of having different results.

The elastic impedance models resulted in low frequency inverted model as compared to the acoustic impedance inverted model with all the inversion techniques applied. The lithology can be distinguished better from the acoustic impedance model than elastic impedance inverted model.

Chapter 6: Conclusion

In this study, an effort has been made to characterise the Gullfaks reservoir for lithology identification. To achieve this purpose, post-stack seismic inversion was done, as the available data was full-stacked 3D seismic cube with check shot surveys. After the quality control of the available well log data, only one check shot survey was selected to use in the inversion process.

On the basis of obtained results following conclusions can be drawn.

- The seismic pseudo logs can give very useful lithology information. Correlation with the well logs improves the accuracy and helps in identifying the facies change at the large distance from the well location. The accuracy of the impedance logs depends upon the amplitude scaling and high and low frequency information. The proper selection of wavelet is also very important. Apart from this, good quality well logs data with correct elevation is required to make the synthetic seismic trace, particularly in the reservoir zone.

- Post-stack seismic inversion proved to be a useful method to understand the subsurface reservoir. On the basis of results showed in chapter 5, acoustic inverted models showed more reliable and detailed results than elastic impedance inverted models at zero offset. It was also considered to change the initial models with each other to re-check the results, but it was not possible to perform.

- Four different inversion algorithms were used to invert the acoustic and elastic impedance models. It was found from the results, that Bandlimited algorithm is the most robust one as it generates more detailed results than the other inversion algorithms. The sparse spike algorithms produced less detailed results than the other two approaches. All these algorithms need to be constrained carefully to deal with non-unique results.

Chapter 7: Future Recommendations

On the basis of current research work following recommendation has been made for future work.

- Using the pre-stack seismic data, an inversion model at zero offset can be built. The obtained results can be compared with the results from post-stack seismic inversion using elastic impedance model with zero offset. This will give a clear picture that is it possible to use full-stack data to make the elastic impedance model or there is certain problem in initial model building for post-stack seismic inversion.

References

Badley, M. E., Price, J. D., Dahl, C. R., & Agdestein, T. (1988). The structural evolution of the northern Viking Graben and its bearing upon extensional modes of basin formation. Journal of the Geological Society, 145(3), 455-472.

Badri, M., M. Svendsen and M. Egan, (2002). Reducing drilling risk through improved seismic imaging. utilizing new signal-sensor acquisition technology: AAPG Annual International Meeting, Cairo, Egypt.

Barclay, F., Bruun, A., Rasmussen, K. B., Alfaro, J. C., Cooke, A., Cooke, D., & Roberts, R. (2007). Seismic Inversion: Reading Between the Lines.

Erichsen, T., Helle, M., Henden, J., & Rognebakke, A. (1987). Gullfaks. Geology of the Norwegian oil and gas fields: London, Graham and Trotman, 273-286.

Fact Pages Norwegian Petroleum Directorate, synchronized 12.09.2013. Reserves, retrived May, 2013. http://factpages.npd.no/factpages/Default.aspx?culture=en.

Fossen, H., & Hesthammer, J. (1998). Structural geology of the Gullfaks field, northern North Sea. SPECIAL PUBLICATION-GEOLOGICAL SOCIETY OF LONDON, 127, 231-262.McClay et al. 1986.

Fossen, H., & Rørnes, A. (1996). Properties of fault populations in the Gullfaks Field, northern North Sea. Journal of Structural Geology, 18(2), 179-190.

Hesthammer, J., & Fossen, H. (2001). Structural core analysis from the Gullfaks area, northern North Sea. Marine and Petroleum Geology, 18(3), 411-439.

Gabrielsen, R. H., Færseth, R. B., Steel, R. J., Idil, S., & Kløvjan, O. S. (1990). Architectural styles of basin fill in the northern Viking Graben. Tectonic Evolution of the North Sea Rifts. Clarendon Press, Oxford, 158-179.

Gardner, G. H. F., Gardner, L. W., & Gregory, A. R. (1974). Formation velocity and density-the diagnostic basics for stratigraphic traps. Geophysics, 39(6), 770-780.

Latimer, R. B., Davidson, R., & Van Riel, P. (2000). An interpreter's guide to understanding and working with seismic-derived acoustic impedance data. The leading edge, 19(3), 242-256.

Lindseth, R. O. (1979). Synthetic sonic logs-a process for stratigraphic interpretation. Geophysics, 44(1), 3-26.

Mondol, N, H., (2003). Reservoir prediction through 3D seismic interpretation and post-stack seismic inversion – An integrating approach to reveal reservoir properties in Gullveig Field, northern North Sea. Master dissertation at Norwegian University of Science and Technology, 32-36.

Pendrel, J. (2001). Seismic inversion–the best tool for reservoir characterization. CSEG Recorder, 26(1), 18-24.

Pendrel, J., & Van Riel, P. (1997). Methodology for seismic inversion and modeling: A western Canadian reef example. CSEG Recorder, 12(5), 5.

Petterson, O., Storli, A., Ljosland, E., & Massie, I. (1990). The Gullfaks field: geology and reservoir development (pp. 67-90). Springer Netherlands.

Roberts, A. M., and G Yielding. (1995). Continental extension tectonics, in hancock, P. L. (ed) New concept in tectonics, Pergamon, Oxford.

Russell, B., & Toksöz, M. N. (1991, November). Comparison of poststack seismic inversion methods. In 1991 SEG Annual Meeting.

Shrestha, R. K., & Boeckmann, M. K. (2002, October). Stochastic seismic inversion for reservoir modeling. In 2002 SEG Annual Meeting.

Treitel, S., & Robinson, E. A. (1966). The design of high-resolution digital filters. Geoscience Electronics, IEEE Transactions on, 4(1), 25-38